DOE/CH/10201--T3

DOE/CH/10201--T3

DE93 002846

Department of Energy

Grant No. DE-FG02-84CH10201

MAXIMALLY CONCENTRATING OPTICS FOR PHOTOVOLTAIC SOLAR ENERGY CONVERSION

TECHNICAL PROGRESS REPORT

Submitted: March 7, 1985

Principal Investigators:

Joseph J. O'Gallagher

Roland Winston (Correspondent)

The University of Chicago

The Enrico Fermi Institute

5640 S. Ellis Avenue

Chicago, Ill. 60637

TABLE OF CONTENTS

ABSTRACT

Use of a two-stage concentrator with a fresnel lens primary and a nonimaging dielectric totally internally reflecting secondary, has unique advantages for photovoltaic concentration. Some preliminary ray trace studies have shown that with planar lenses, an increase in angular acceptance for a given geometric concentration to about 2/3 of the maximum theoretical limit can be achieved. To demonstrate this, two preprototype concentrators, each having a geometric concentration of 248:1 for a 0.635cm (0.25 inch) diameter cell, have been designed, built, and tested. Measurements of the angular response show an acceptance of 8° (full angle) which is dramatically better than the 1°-2° achievable without a secondary, and is in excellent agreement with the ray trace predictions. For these preprototypes, passive cooling was sufficient to prevent any thermal problems for both the cell and secondary. No problems associated with nonuniform cell illumination were found, as evidenced by the fill factor of 71%-73% measured under concentration. Initial measurements of the system electrical efficiency lie in the range 7.5%-9.9% for a variety of individual cells. Research is continuing to reduce residual optical losses with improved system efficiencies approaching 12% expected to be achieved with good cells. A third preprototype configuration is under development, and construction and evaluation of operating a multi-element prototype is planned for the next phase.

I. Introduction

A. Background

This report describes research efforts to develop two-stage nonimaging concentrators for solar photovoltaic applications carried out at the University of Chicago from July 1, 1984 through January 31, 1985. This period covers the first seven months of a one-year grant awarded by the Department of Energy under the Soleras program. An accompanying renewal proposal outlines a continuing program and seeks support for further development of the concept which is expected to lead to an operating multielement prototype.

The goal of the project is to use the techniques of nonimaging optics (1) to design totally internally reflecting (TIR) transparent dielectric secondary elements which are optimally matched to a fresnel lens primary for a given solar cell. The technique is described in the original proposal (2) and some previous papers (3,4) by our group. The secondary acts to spread the focused sunlight more uniformly across the surface of the cell and to increase greatly the effective intercept area of the cell (by factors of 10-15) in the focal plane of the primary lens. The latter effect dramatically increases the angular pointing tolerance for a particular cell-primary combination. As illustrated in two figures from the original proposal, the secondary can be used either to design very high concentration systems with relatively high tracking tolerances -- for example, approaching 1000:1 in the ideal limit -- with $\pm 2°$ (Figure 1) or intermediate concentration levels, e.g. 100:1 approaching (in the limit) $\pm 8°$ tolerances (Figure 2). The secondaries belong to the family of so-called nonimaging optical devices which includes the more familiar Compound Parabolic Concentrator (CPC). For reasons having to do with the limiting

shape of the sidewall profile, the type used here is referred to as a Dielectric Compound Hyperbolic Concentator or DCHC. This is the first systematic study of these techniques for photovoltaic concentrators, and the objectives are to investigate the practical problems involved e.g., optical coupling, thermal effects, practical performance limitations, etc., through the design, test and evaluation of preprototype designs.

B. Summary of accomplishments

To date we have designed, built, tested, and analyzed two different lens concentrator systems. Each has the same overall geometric concentration ratio of 248:1, but different secondary designs have been employed. These preliminary measurements demonstrate the improvements that can be achieved with these types of designs, in that the angular acceptance for both designs is close to 8°(FWHM) as compared with practical limit of 1°-2° with no secondary. The electrical performance of the cell under full concentration is very good with a fill factor of 74% and system efficiency of 9.9% achieved so far. This indicates that there are no detrimental effects associated with non-uniform intensity distribution on the cell. The optical transmission efficiency of the secondaries is in the range 84-91% which is slightly less than predicted (90-95%) but is expected to be improved upon in subsequent designs. This work has demonstrated the feasibility of the approach and revealed a number of technical areas requiring further study. We are in the process of developing a third preprototype configuration to implement these studies and to serve as the baseline configuration for the multi-element prototype proposed for the next phase. The details of the overall research are given in the following sections.

II. Conceptual Design Studies

A. Preliminary ray trace studies

Before selecting a particular design to build and evaluate, a preliminary study of a reference configuration was carried out. This was similar to the high concentration concept shown in Figure 1, and consisted of a 10-inch-diameter fresnel lens combined with a 0.25-inch-diameter cell. This corresponds to a geometrical concentration C_{geom} of 1600X for a circular primary (or ~1000X for a square primary of 10" diagonal). The "thermodynamic limit" for the angular acceptance for this concentration and a dielectric refractive index, n, is

$$\theta_p = \text{Sin} \frac{n}{\sqrt{C_{geom}}} \qquad (1)$$

or, in this case, $\theta_p = \pm 2.15°$. We chose a secondary with an acceptance angle of $\pm 22°$, slightly more than is necessary to accomodate a f/1.45 lens. This, together with the choice of a 120° arc for the secondary front curved surface, fixes the secondary design. The corresponding entrance aperture of 0.92" reduces the maximum achievable acceptance angle to somewhat less than $\pm 2°$. Figures 3 and 4 are ray diagrams for incidence angles $\theta_i = 0°$ and 1°, respectively, relative to the lens normal. These assume a point source and constant index of refraction (n = 1.49). In each figure, (a) is an overall ray diagram in the meridian plane, (b) shows a close-up of the secondary, and (c) shows the ray patterns projected into the secondary entrance aperture and exit aperture planes. The effect of aberrations on the fresnel lens in smearing out the focus for off-axis incidence is clearly seen at 1°. However, at $\theta_i = 1.5°$ some rays begin to miss the secondary (Figure 5a), and by 1.75° this results in intercept losses of about 50% (Figure 5b). This

limits the achievable response with a flat fresnel lens to about 2/3 of that for an "ideal" lens (one satisfying the Abbe Sine condition on off-axis imaging). In principal, it could be improved by introducing correction in the lens by, say, curving the front surface. However, for this phase we limited our choice of lens to planar lenses. The over-all geometrical throughput as a function of θ_i for this conceptual design configuration calculated from ray tracing is shown in Figure 6. An "ideal" lens with this secondary would have a sharp cutoff at $\pm 1.92°$. The planar fresnel lens has a rounded gradual fall-off which is 90% at $\pm 1.4°$. Geometrical losses in the secondary DCHC are negligible. For comparison, the throughput to a 1/4" cell is shown both for an "ideal lens" and for a planar fresnel lens. The improvement due to the secondary is a factor of 3.5 in angular tolerance.

B. Practical design considerations

The geometrical angular response shown in Figure 6 is for a point monochromatic source. The sun's disk subtends an angular cone of ± 4.6 milliradians (0.26°), and the variation in refractive index for acrylic over the relevant portion of the solar spectrum is ± 0.01 out of 1.49. This can be represented as an effective angular divergence of ± 6.7 milliradians (0.38°). The combined result of these two effects consumes nearly half the achievable tolerance for the high concentration reference design. On the other hand, these effects are much less important in a lower concentration region. Furthermore, temperature and intensity distribution effects will be much less severe at lower concentrations. Finally, we note that cells capable of operating under ~1000 suns are still under experimental development whereas standard silicon concentrator cells for

operation under 100 to 300 suns are readily available. For all of the above reasons it was felt that the first operational preprototype for our measurements should be built for the lower concentration region, and the remainder of this report is concerned with this application.

III. Preprototype Design and Assembly

Profile drawings of the two-stage configurations selected for experimental evaluation are shown in Figures 7 and 8. Each consists of a 0.25" (0.635cm) diameter cell with a 10cm diameter flat fresnel lens corresponding to a geometric concentration ratio of 248X. The secondary for what we refer to as MOD-A is identical to that used in the conceptual design configuration discussed above. The version designated MOD-B has a secondary with the same acceptance angle ($\pm 22°$) and exit aperture as that for MOD-A but a front surface curvature of half arc equal to the acceptance angle.

In each case the cell has been mounted on a one-inch-diameter, 2mm-thick copper heat sink. This in turn is mechanically mounted and thermally coupled with heat conducting compound to a three-inch-square black anodized aluminum plate with 1/4" fins to further dissipate any thermal loads.

The secondaries were optically coupled to the solar cell surface with silicon compound and mechanically supported by means of a positioning ring designed to grip the secondary at its widest point. This ring was then mounted to the heat sink base. The entire assembly was made so that the secondaries can be mounted and de-mounted in a short time, enabling reference measurements on the bare cell to be carried out in between secondary performance measurements.

IV. Preprototype Testing and Evaluation

A. Secondary performance

The optical performance of each secondary was measured in terms of the short circuit current gain. That is for a cell of Area A_c if we define the normalized current density j as

$$j = \frac{i_{ss}(t)}{A_c \cdot I_c(t)} \tag{2}$$

where $i_{ss}(t)$ and $I_c(t)$ are the short circuit current and insolation seen by the cell at time t. We then define the current gain G as the ratio of normalized current density with secondary in place to that for the bare cell. Then for a secondary with geometric concentration C_2 the optical efficiency is

$$\eta_2 = G/C_2 \tag{3}$$

which is measured as a function of angle of incidence.

The measured angular response for the MOD-A secondary is plotted in Figure 9. It shows a broad pedestal shape with corners slightly rounded relative to the "ideal" rectangular response. The latter has sharply defined cut-offs characteristic of the geometrical throughput function (i.e. calculated without losses from reflection, absorption, etc.). Full width at half maximum is 44°, conforming precisely to the design value of $\pm$22°. The average optical efficiency across the flat portion is $\eta_{2,A} = 87.5 \pm 2\%$. The two percent uncertainty is typical of the variation in measurements taken in Chicago under the real sun on different days and is largely due to uncertainty in the correction for contributions of diffuse sunlight to the bare cell response. The $\pm$18.4° angular cone subtended by the 10cm primary lens seen from its focus is indicated.

The data in Figure 9 show somewhat more rounded "shoulders" and a slightly lower average throughput than should be achievable. These data are replotted in Figure 10, superimposed on a series of curves from ray trace calculations for the MOD-A DCHC. Successively lower curves show the effect of including losses due to reflection at the front curved surface, reflection losses at the dielectric cell interface, absorption losses in the acrylic, and a small loss due to TIR "leakage". Including all these losses does describe the average values observed, but the calculated curves do not reproduce the observed "rounding". We are still carrying out further measurements to isolate the individual loss mechanisms and reduce their effect. One area of expected improvement is in the optical interface between the secondary and the cell. We have not tried to optimize the match between the indices of refraction of acrylic and silicon to minimize reflection losses. On the basis of both calculation and previous experience in a program at Argonne National Laboratory, efficiencies in the range 90-94% should be achievable.

Figure 12 shows the measured angular response curve for MOD-B. It is very similar to that for MOD-A except that the average throughput is somewhat lower corresponding to $\eta_{2B} = 84 \pm 2\%$. This indicates that there is a component to the optical losses that depends either on height (i.e. absorption) or surface area (i.e. TIR). These effects are stil under study. In any case, these results indicate that the shorter, smaller DCHC with sharper lens curvature is the preferred design.

B. Performance of the full concentrator (lens plus secondary)

The angular response function measured in terms of the short circuit current for the continued Lens/DCHC is shown for three different

lens-secondary spacings in Figure 12. The best performance in both throughput and width corresponds to the nominal focal length of 15cm. The measured angular width at 90% of maximum is $\pm 3.5°$ ($\pm 4°$ at half-maximum) which, as expected, is about 2/3 of the ideal limit. The measured efficiency for the fresnel lens by itself is $\eta_1 = 81 \pm 2\%$. This, together with the measured secondary efficiency of 87 $\pm 2\%$, would predict a combined efficiency of $\eta_{12} = 70 \pm 3\%$. The actual combined efficiency calculated from the short circuit current gain is $\eta_{12} = 67 \pm 3\%$, which is close to but slightly lower than predicted. If this is significant, it may be due to the rounding of the secondary angular response function discussed above, and should be improved substantially in future work.

Figures 13 and 14 show ray trace calculations for the shape of the angular response function for MOD-A and MOD-B respectively. The data for MOD-A are also shown and, as is clear, the agreement between the observed width and the predictions is excellent.

C. Preliminary electrical performance

The solar cells used in MOD-A and MOD-B are 1/4" cells on heat sinks selected from a stock of about a hundred such assemblies we have on hand in our own laboratory. They were procured from Microwave Associates as part of an earlier DOE program, and are designed for operation under high concentration in the 100-300 sun range. Typically the short circuit current, open circuit voltage, and fill-factor under one sun are respectively 8.0-9.2ma, 570-600mv, and 70-77%. With $A_c = 0.317 cm^2$, this results in a range of one sun efficiencies from 10% up to nearly 14%. As noted earlier, since we are primarily concerned with optical performance at this stage of the investigation, we have used short circuit

current as the preliminary measure of the system performance, and did not optimize the cell selection to maximize electrical efficiency. We were, however, particularly concerned with how the cells would respond to the de-focused but certainly still somewhat non-uniform intensity distribution emerging from the exit aperture of the secondary under full concentration. Therefore, we carried out a preliminary set of electrical performance measurements under both simulated sun and real sun conditions.

Figures 15-17 are power versus voltage curves for, respectively, a bare cell, the same cell with the MOD-A secondary in place, and finally, the full MOD-A lens/DCHC combination. For these measurements we used an Oriel Optical Mode 6732 solar simulator in our laboratory. This source is a Xenon arc lamp filtered to approximate an Air Mass - 2 spectrum. The output optics collimates the light to approximately $\pm 3°$ which is within (although just barely) the angular response of both MOD-A and MOD-B so that, at least to the first order, no corrections for relative loss of acceptance need be made. Curves for the real sun measurements for the full MOD-B and MOD-A are shown in Figures 18 and 19. These are very preliminary results but two points are worth noting:

(1) The fill factors under both real and simulated sunlight lie in the range 0.71-0.74, which is an indication that there is no serious degradation in cell performance due to non-uniform illumination under a net average concentration of more than 160 suns.

(2) The final net system electrical conversion efficiencies relative to beam insolation lie between 7.5% and 10%. Based on the concentrator optical efficiency, this corresponds to cell efficiencies under concentration between 11.5 and 15%. This implies that, with expected further improvement in secondary optical efficiency to over 90% and a

good cell, overall system efficiencies of 12% should be readily available.

V. Status Summary

Based on a relatively brief effort, we have established that two-stage nonimaging photovoltaic concentrators are easily designed and assembled. We found no major obstacles to their further development: that is, they work. In the moderate concentration range investigated, an acrylic secondary performed quite well and exhibited no serious thermal problems. Using only passive cooling, the cells themselves performed quite well under concentration and exhibited no sign of thermal degradation. This clearly demonstrates that the pointing and alignment tolerances for a given concentration can be increased by a factor of 3 to 4 by the addition of a small inexpensive element. We achieved relatively uniform response over a full cone of 7° (8° at FWHM) for a geometric concentration of 250:1. In general this shows that one can expect to achieve about 2/3 of the thermodynamic limit using planar fresnel lenses (probably more with domed lenses).

Clearly there remain serious unresolved technical issues, and there is much further development needed. Most importantly, a satisfactory explanation for the shortfall of 5-10% encountered in the secondary optical efficiencies needs to be identified and as much of this loss as is possible needs to be recovered. Detailed measurements of the cell electrical performance as a function of secondary placement and alignment need to be carried out. Thermal effects need to be investigated more quantitacively.

We will continue to investigate these questions for the balance of the present grant, using MOD-A and MOD-B supplemented with a third concentrator configuration (MOD-C) using a larger 1cm diameter cell. This future work and a proposed extension is outlined in more detail in the accompanying renewal proposal.

REFERENCES

(1) W.T. Welford and R. Winston, "The Optics of Nonimaging Concentrators," Academic Press, New York (1978).

(2) R. Winston and J. O'Gallagher, "Maximally concentrating optics for photovoltaic solar energy conversion", University of Chicago proposal submitted in response to SOLERAS-84-NPI-001, February 14, 1984.

(3) R. Winston and J. O'Gallagher, "Nonimaging dielectric elements in second-stage concentrators for photovoltaic applications", Solar World Congress; Proceedings of the Eighth Biennial Congress of the Industrial Solar Energy Society, Perth, Australia, 3, 1401 (1984).

(4) J. O'Gallagher and R. Winston, "Development of compound parabolic concentrators for solar energy," Journal of Ambient Energy, 4, 171 (1983).

(5) R. Cole, A.J. Gorski, R.M. Graven, W.R. McIntire, W. Schertz, R. Winston, and S. Swerdling, "Application of compound parabolic concentrators to solar photovoltaic conversion," Argonne National Laboratory, Technical Report ANL-77-42 (1977).

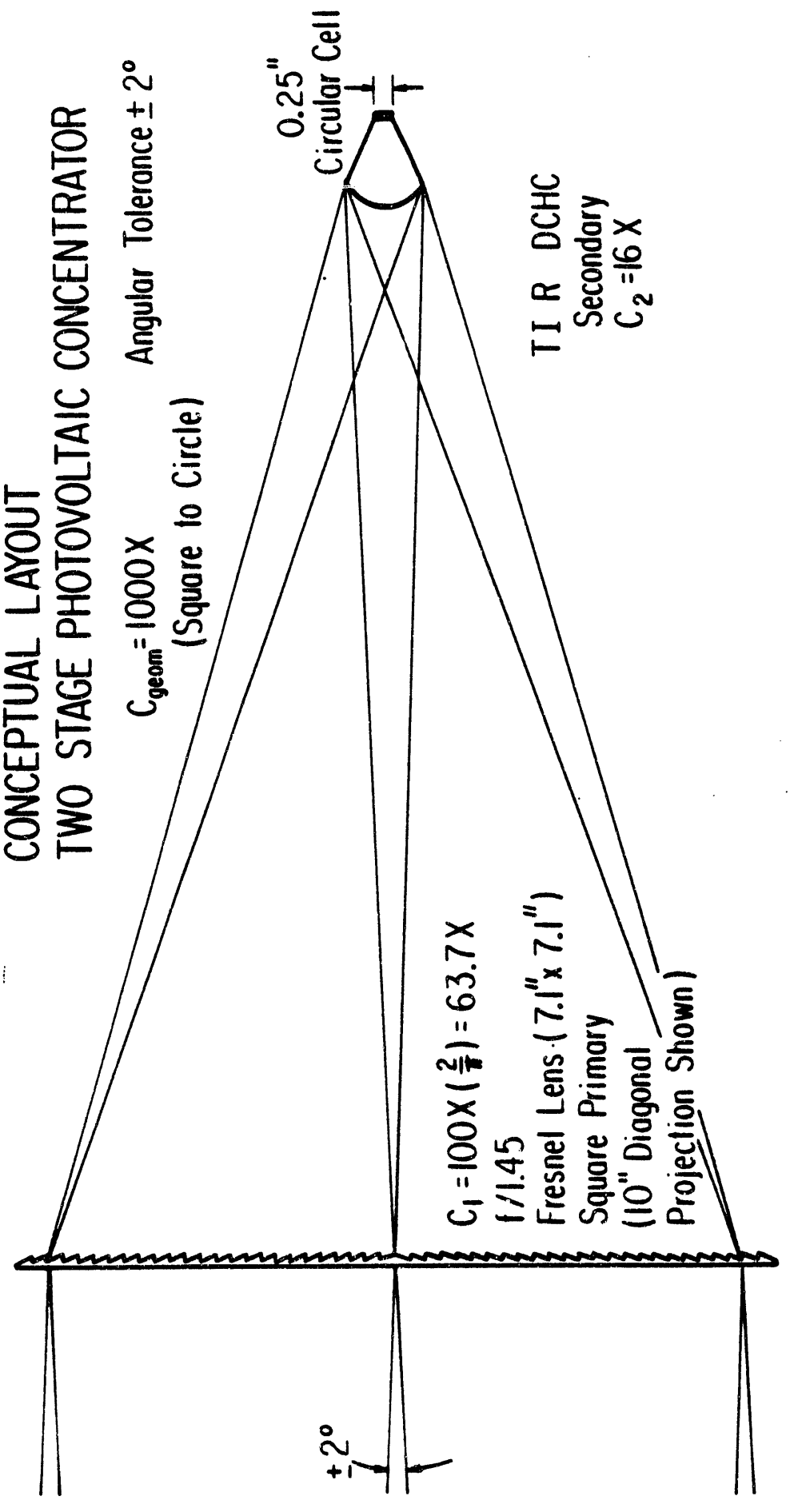

Figure 1. Illustration of high concentration application in the "ideal limit"

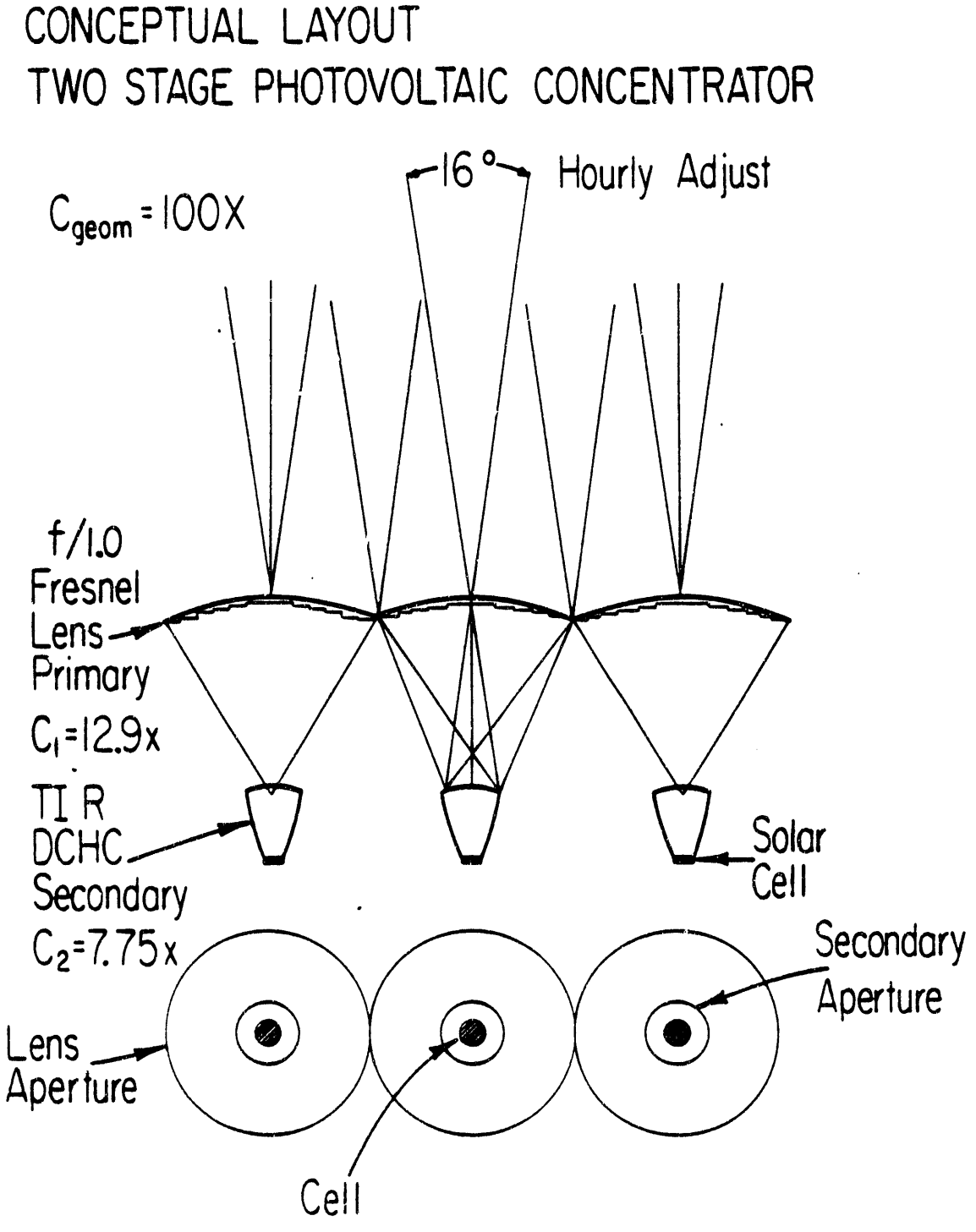

Figure 2. Low concentration "crude tracking" limit

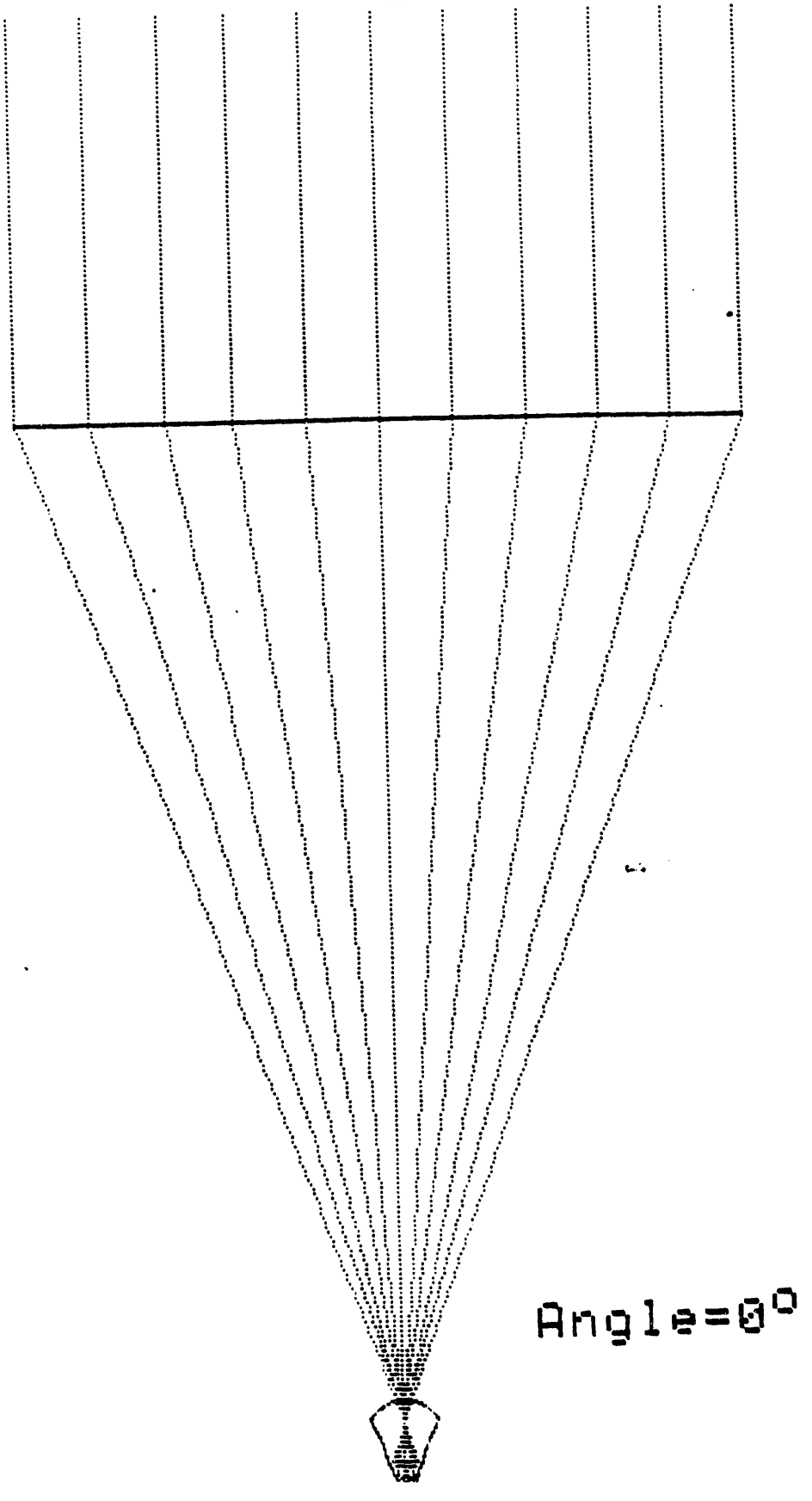

Figure 3a. Ray diagram for 1600X, point source

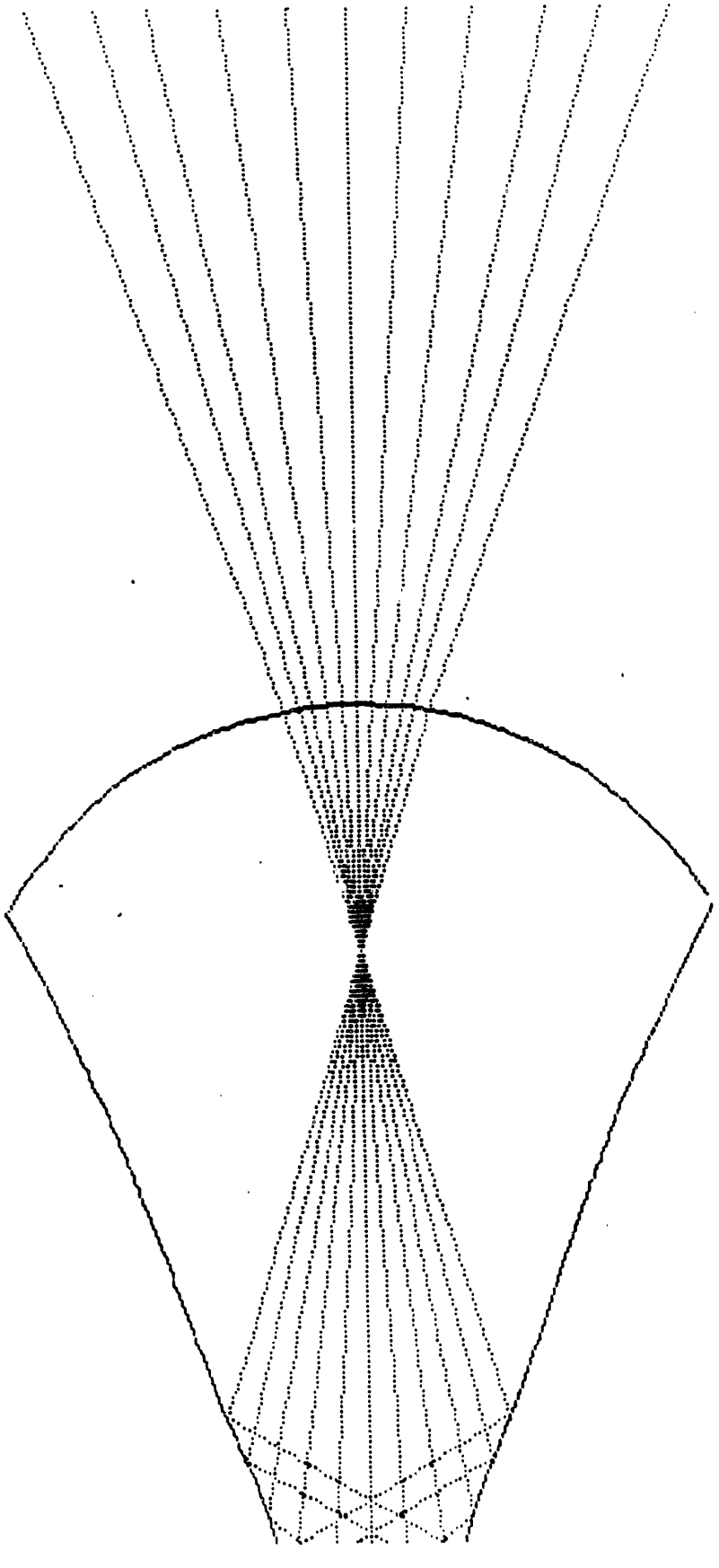

Figure 3b. The DCHC redistributes the flux on the cell

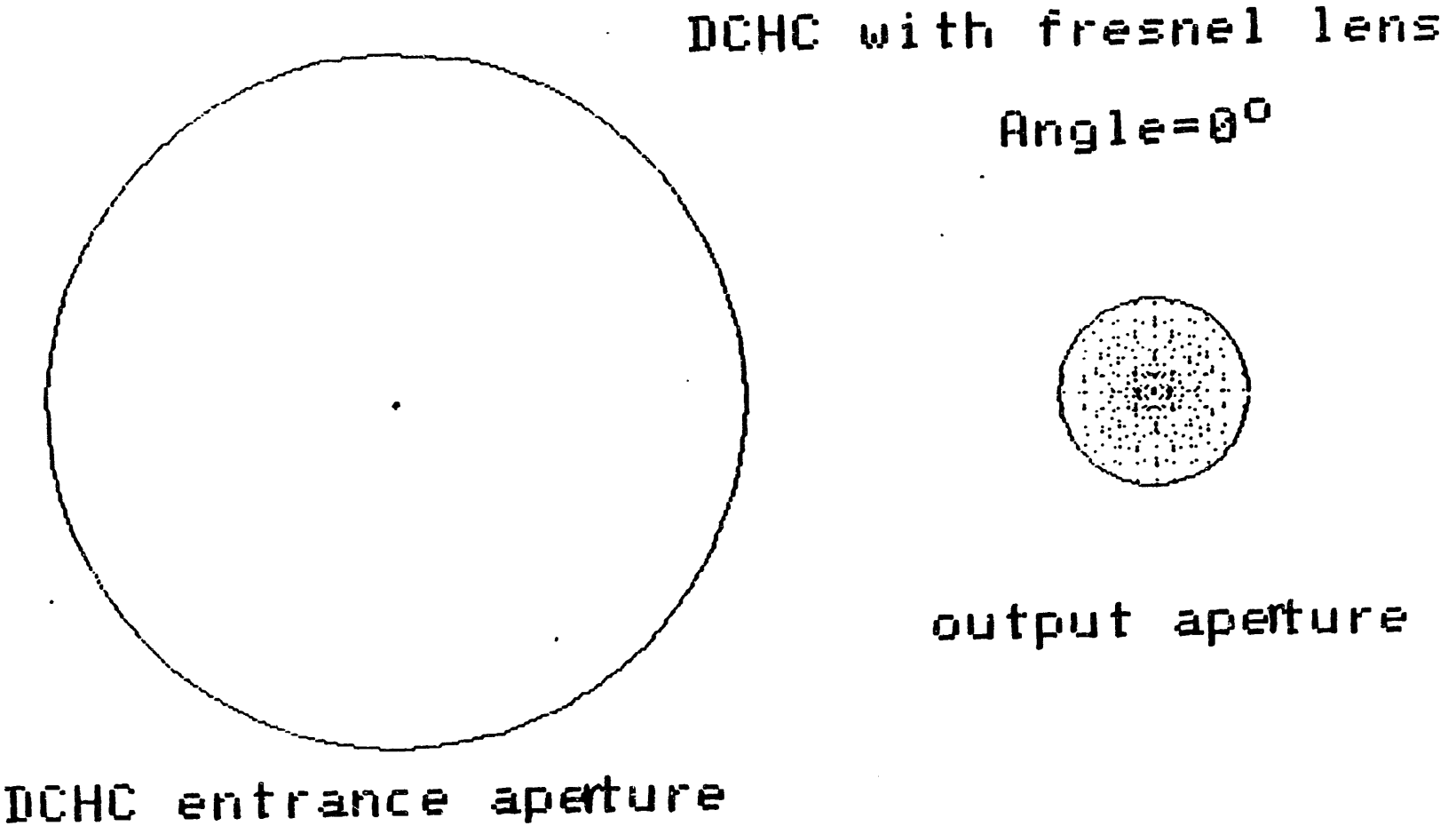

Figure 3c. Projection in focal plane and secondary exit

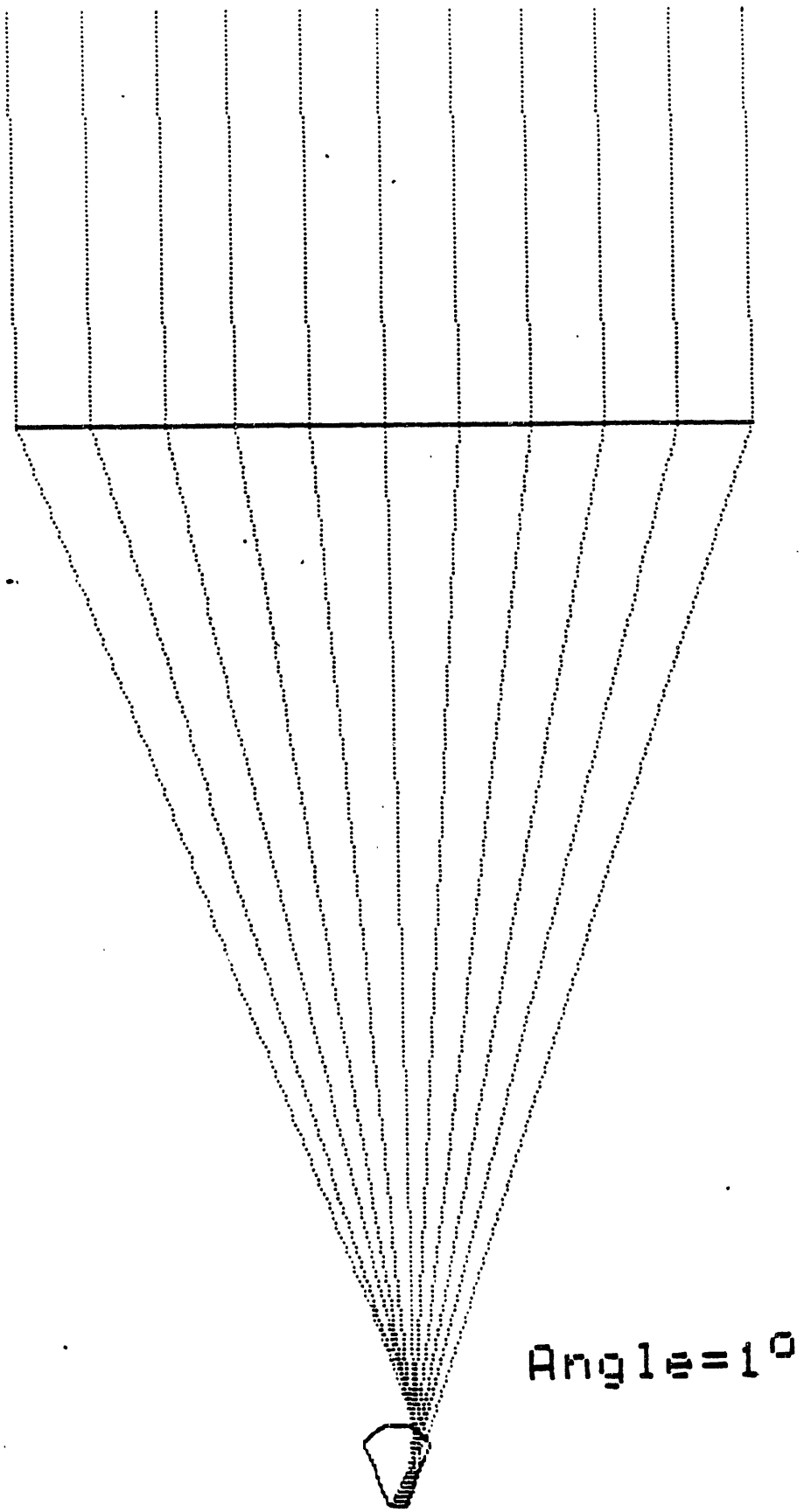

Figure 4a. Ray diagram for 1600X point source at 1° pointing error

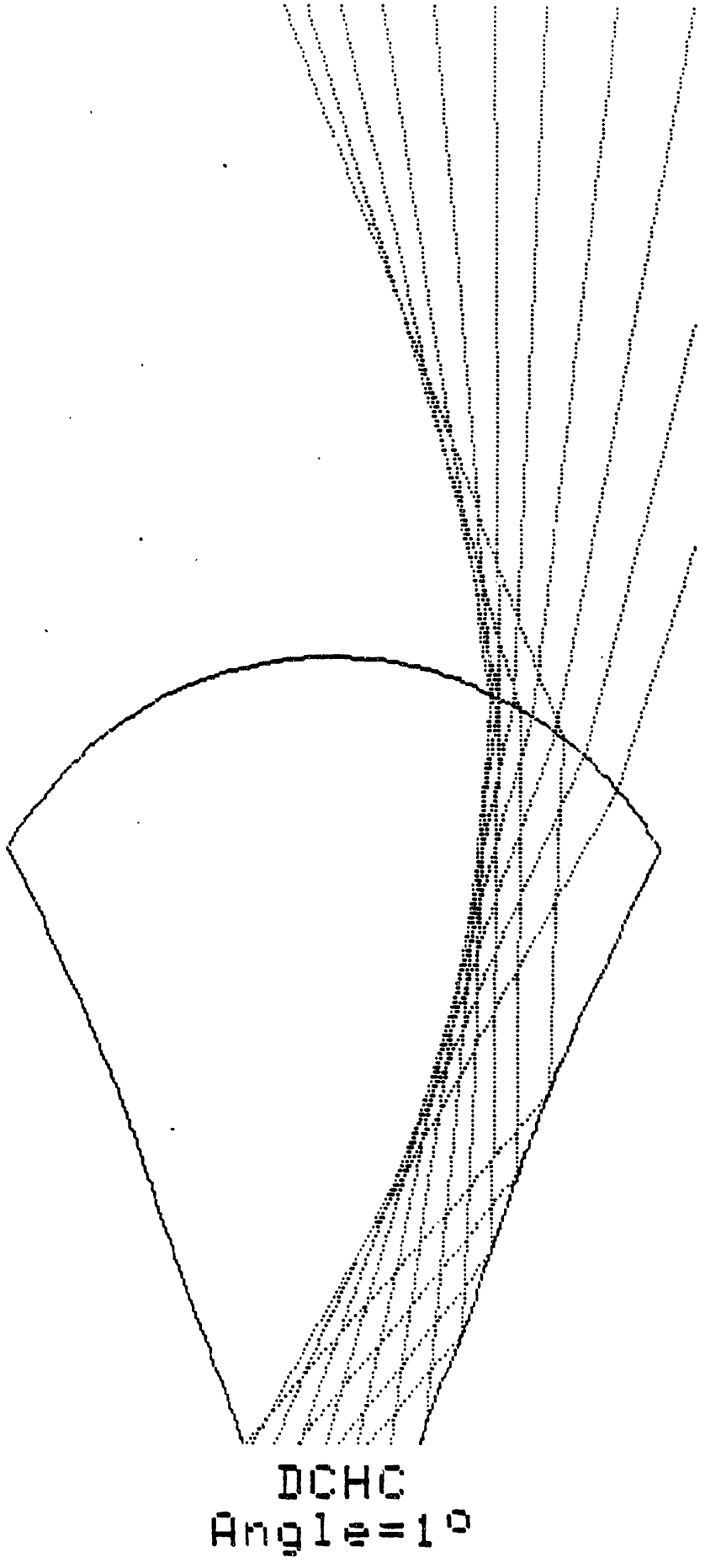

Figure 4b. Aberrations in the primary result in loss of sharp focus even at 1°

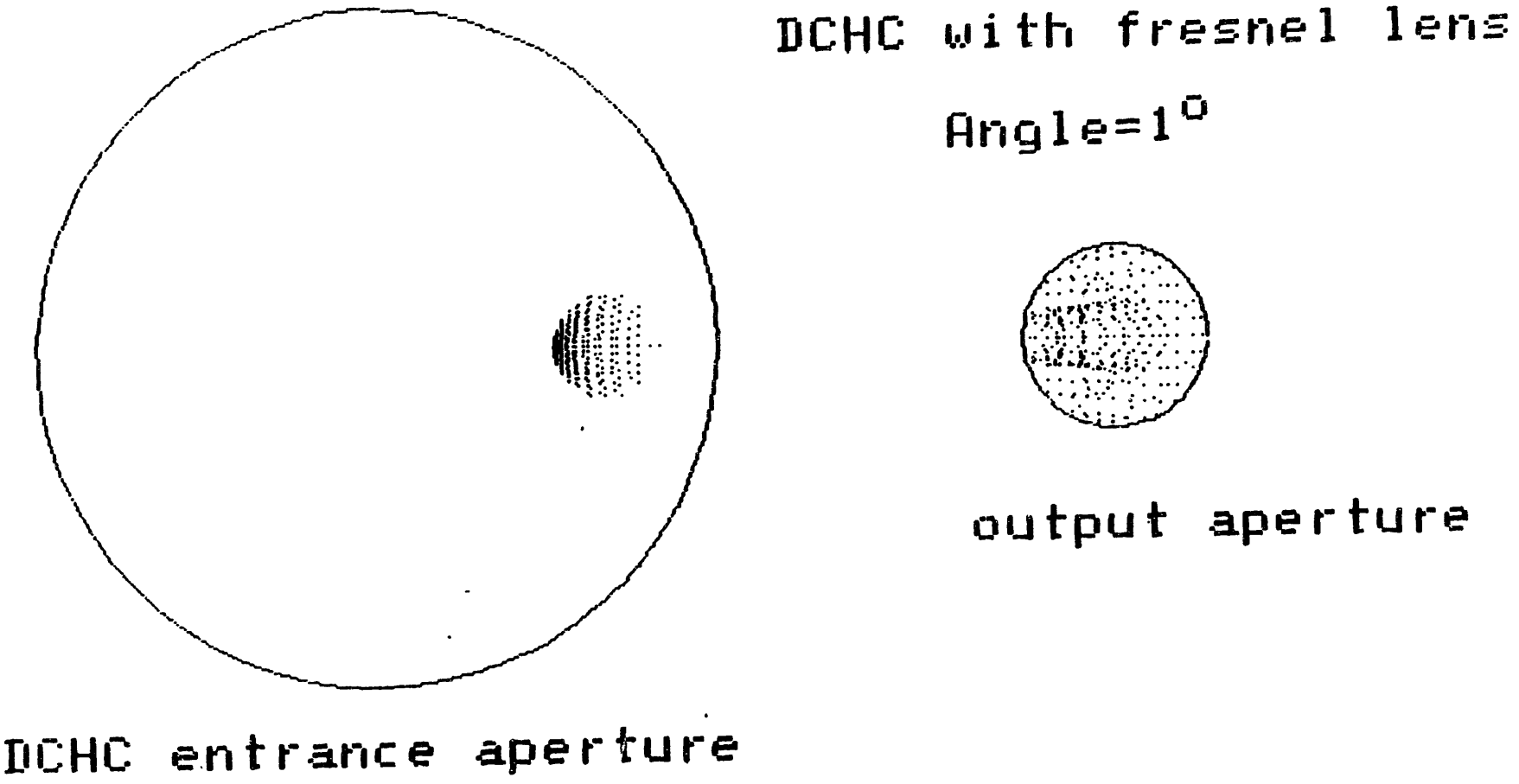

Figure 4c. The secondary still intercepts all the rays at 1°

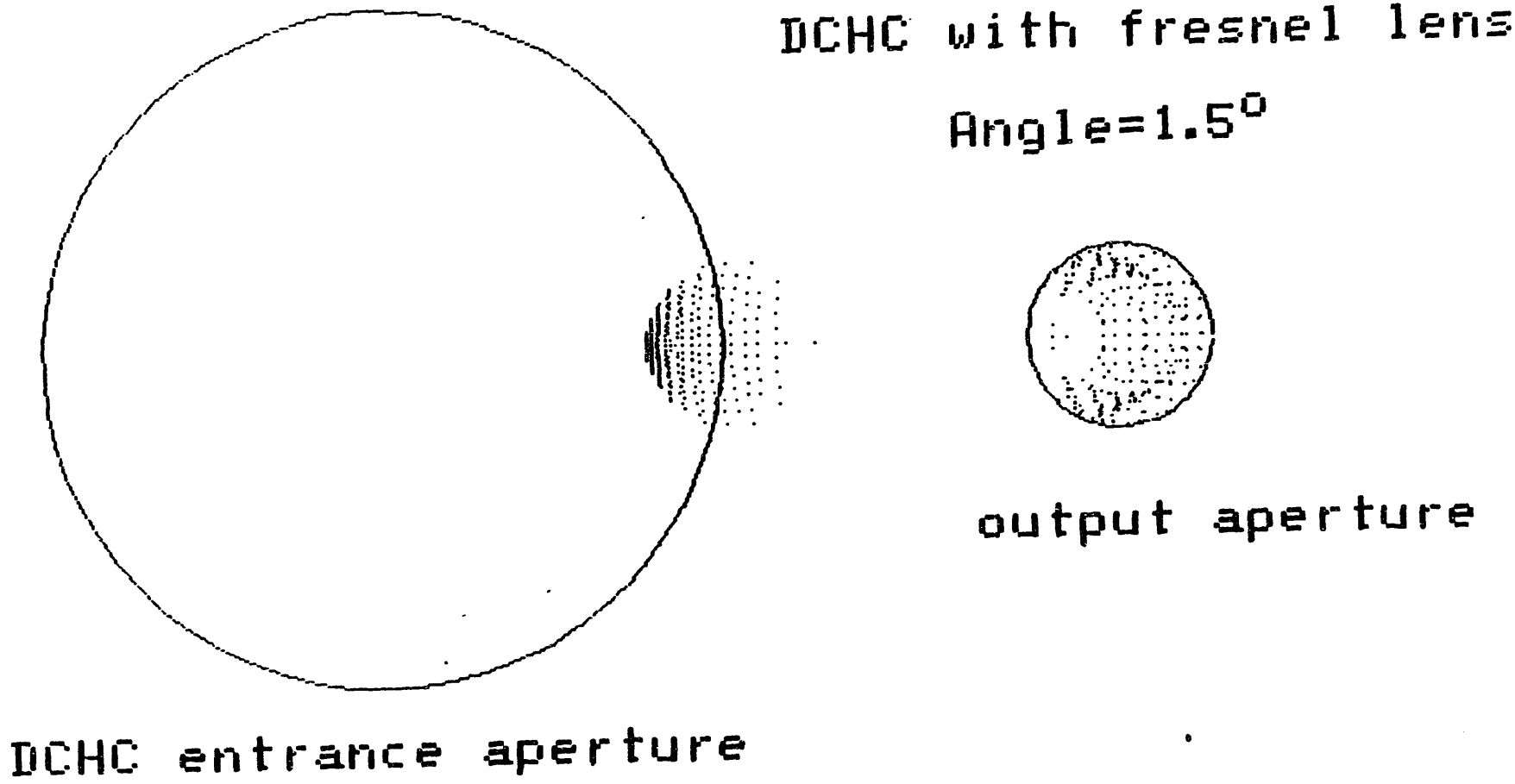

Figure 5a. Some losses begin to occur between 1° and 1.5°

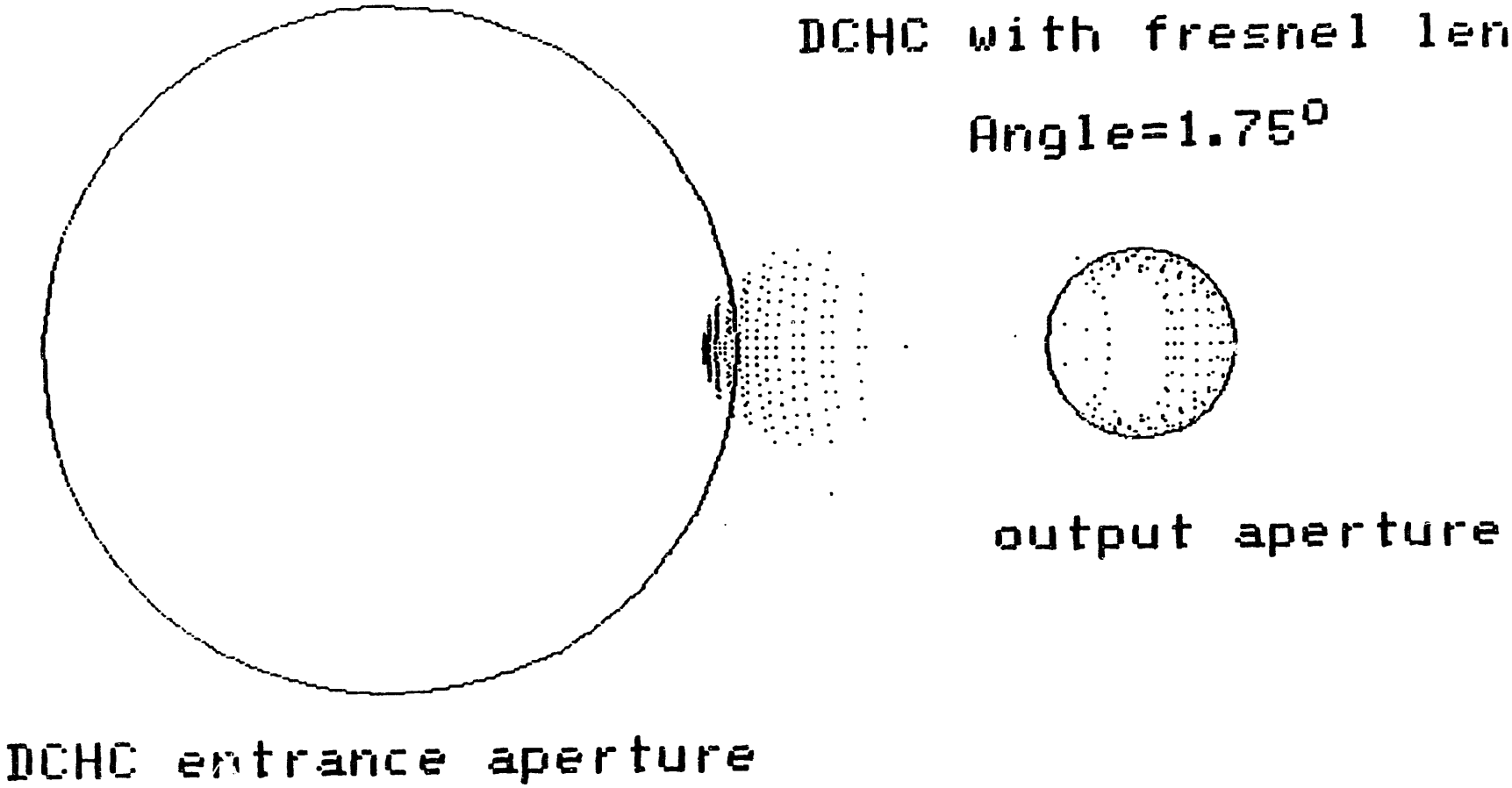

Figure 5b. The losses are prohibitive by 1.75°

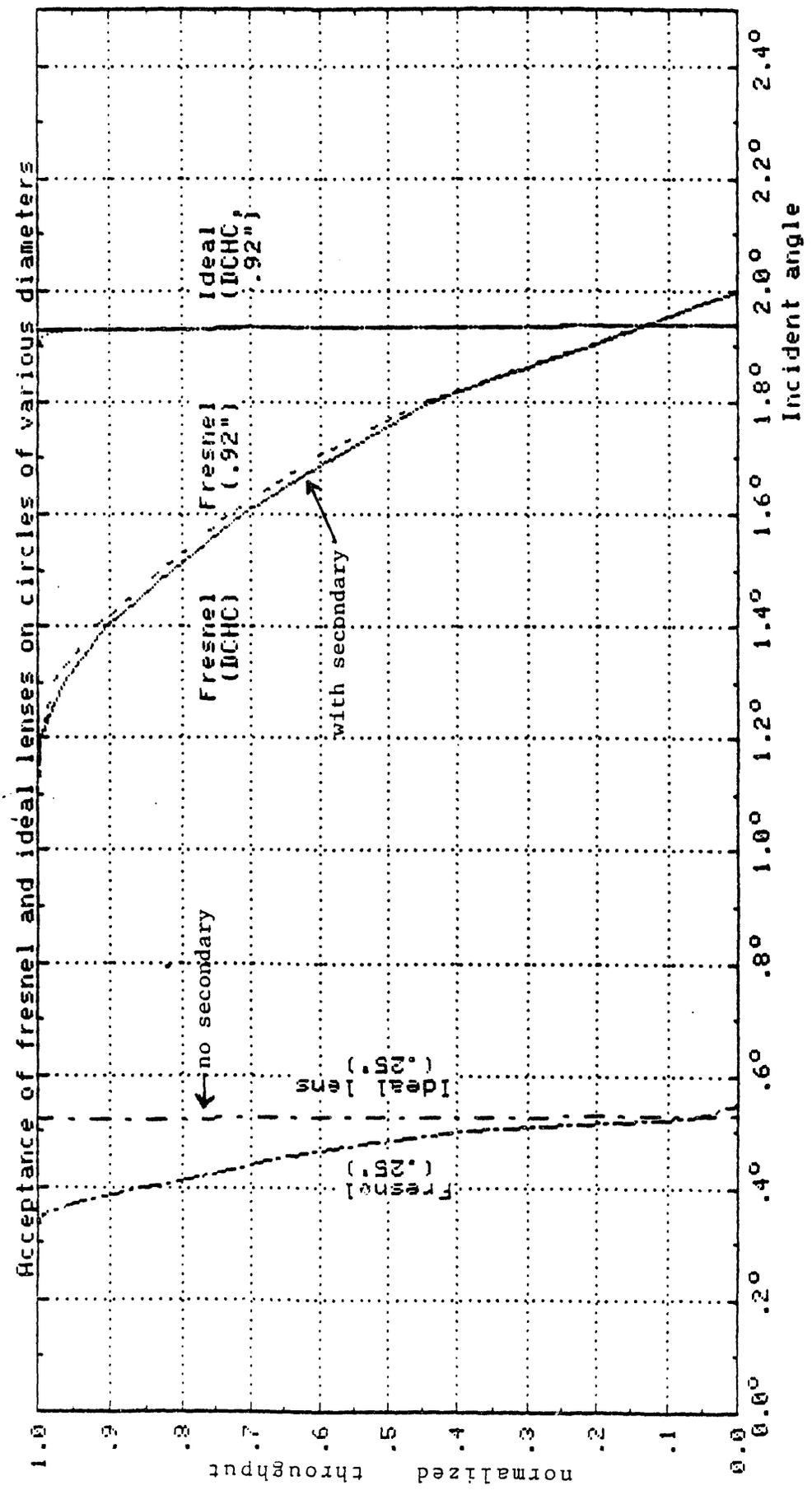

Figure 6. Ray trace calculations of the angular response for a 1600:1 concentrator with and without a DCHC secondary. The aberrations of a flat fresnel lens limit what can be achieved compared with the ideal.

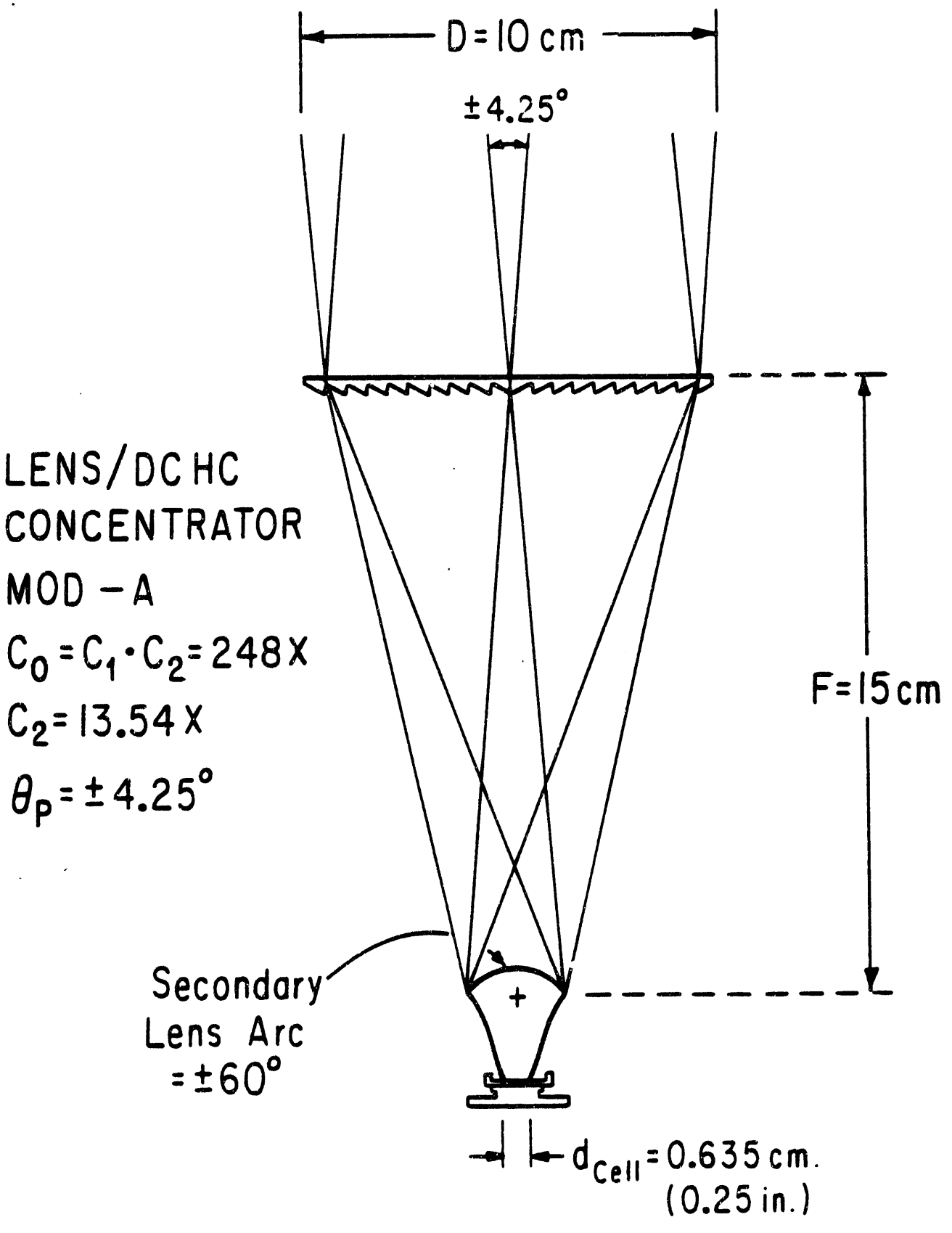

Figure 7. Preprototype two-stage concentrator design profile. The secondary has strong curvature in the front surface.

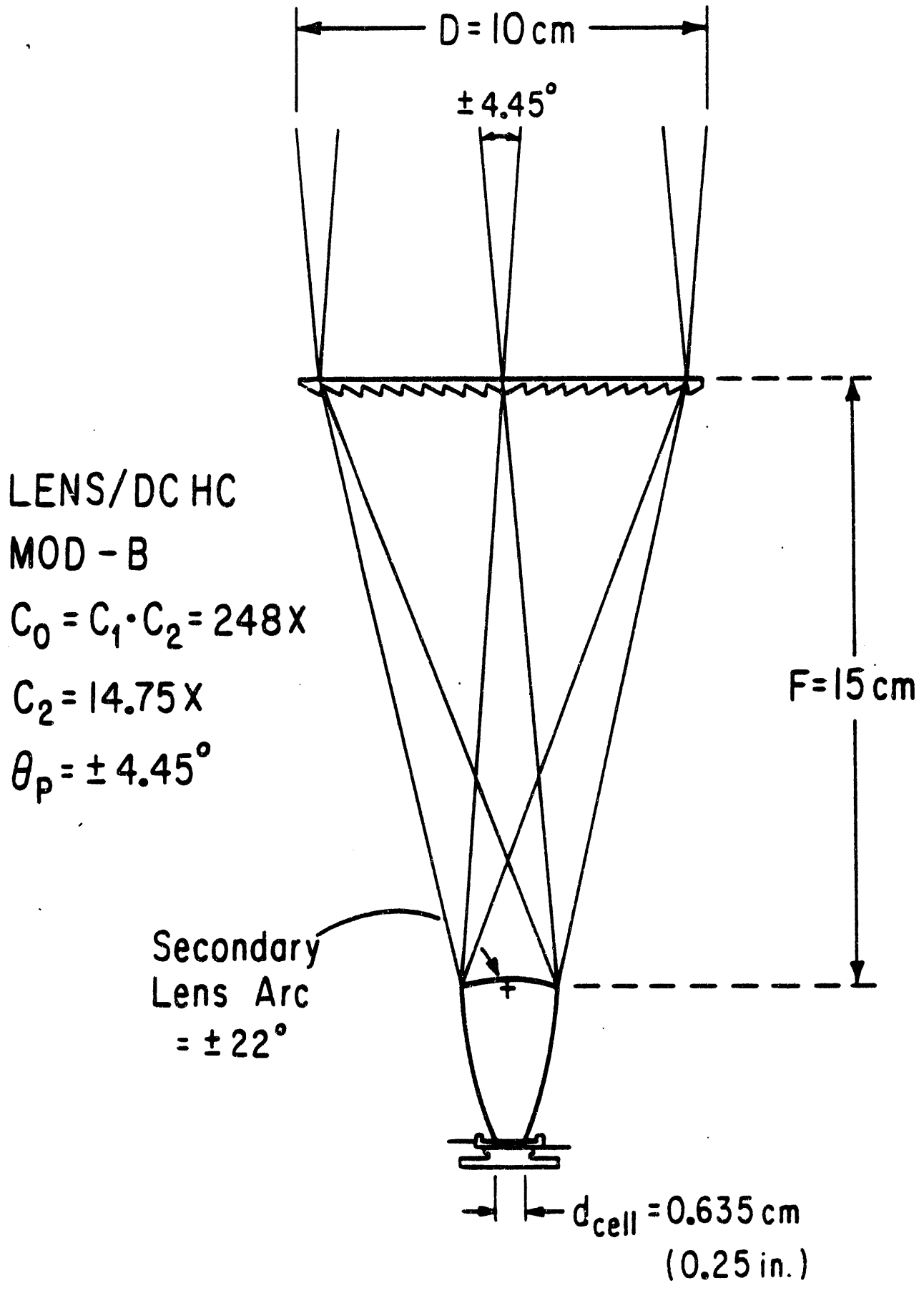

Figure 8. Another two-stage concentrator preprototype. Here the secondary has a softer curvature and more concentration is done by the side walls.

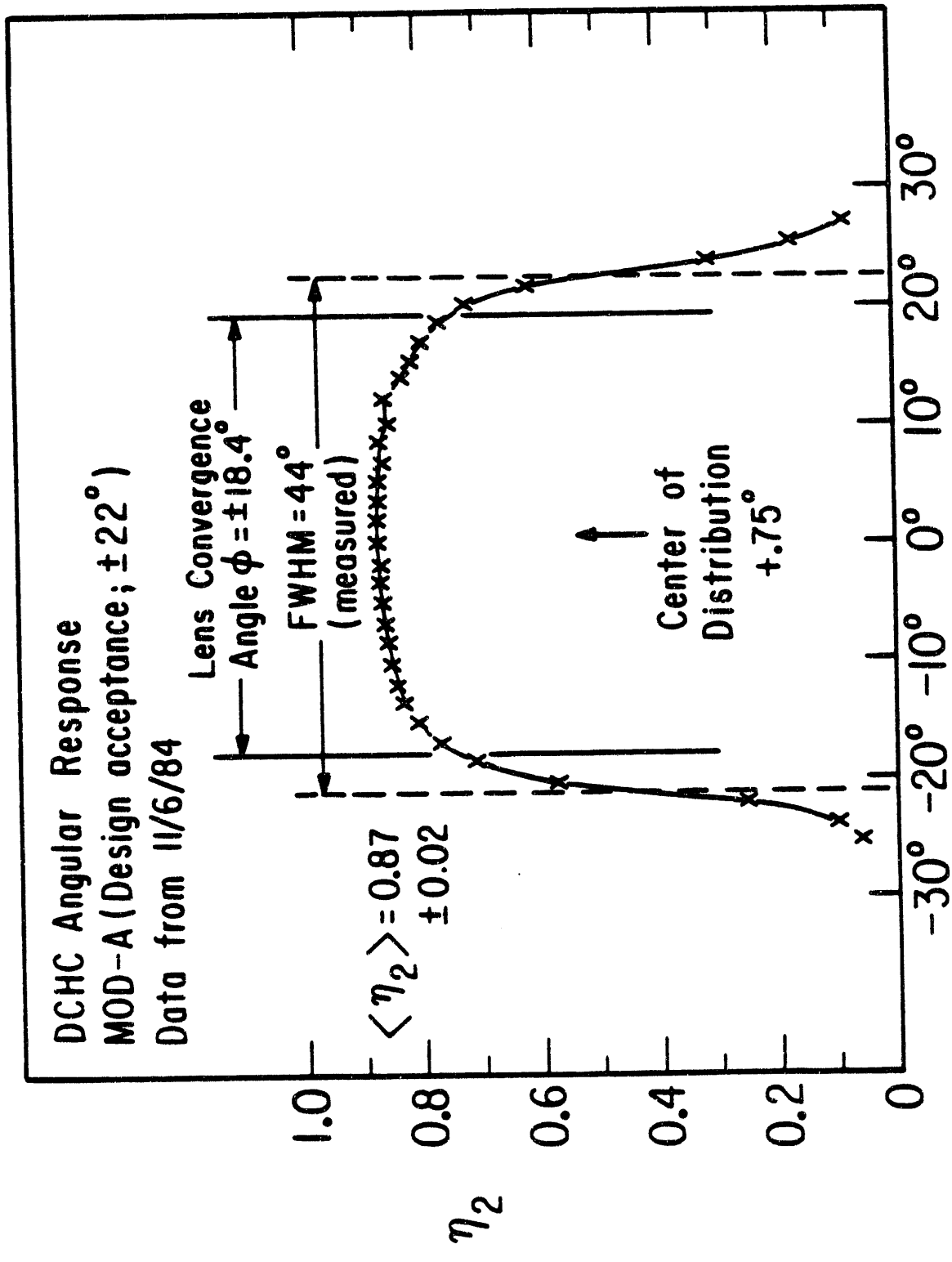

Figure 9. The efficiency as a function of angle measured for the MOD-A secondary

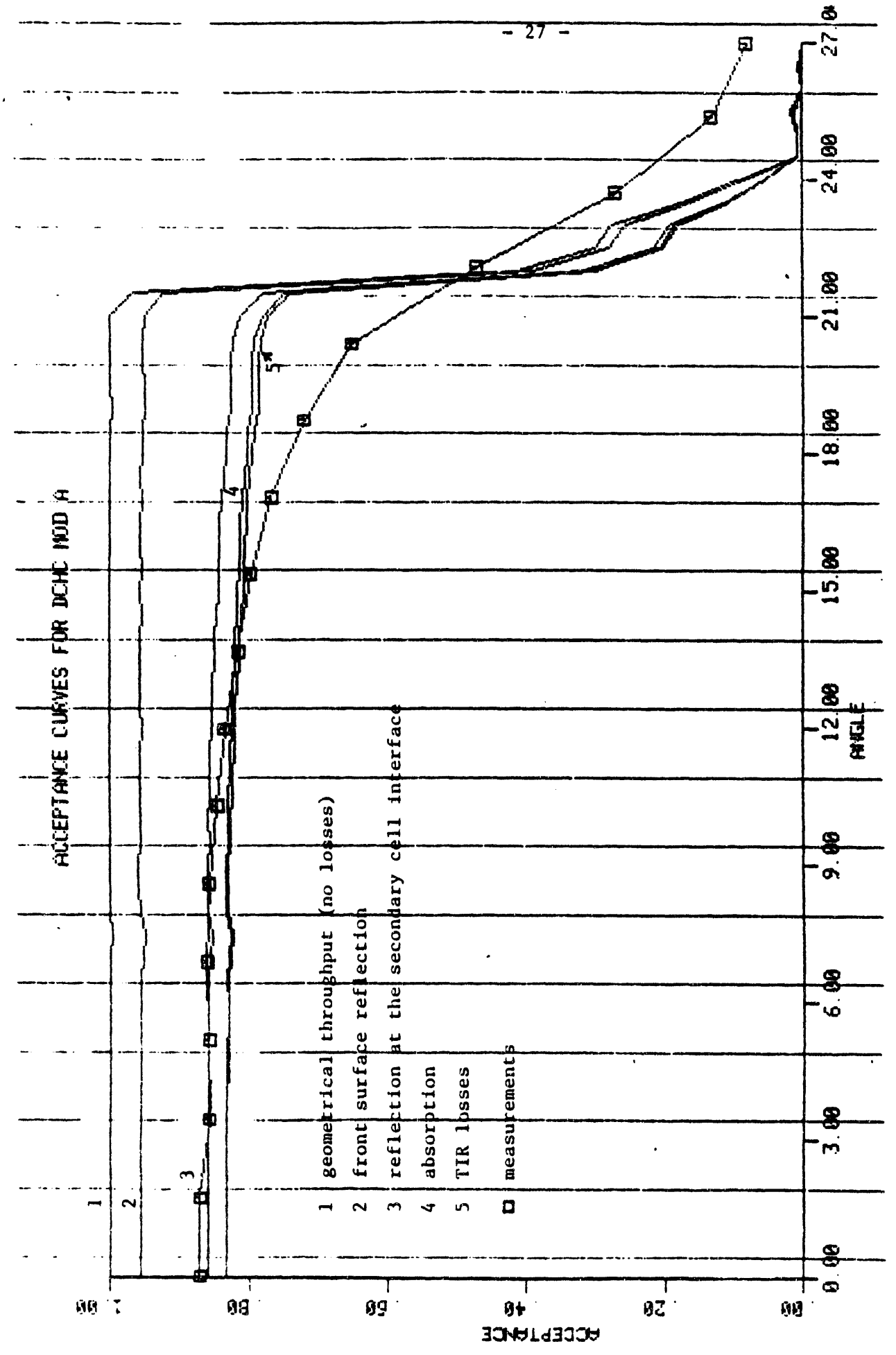

Figure 10. Ray trace calculations of secondary efficiency versus angle compared with observations

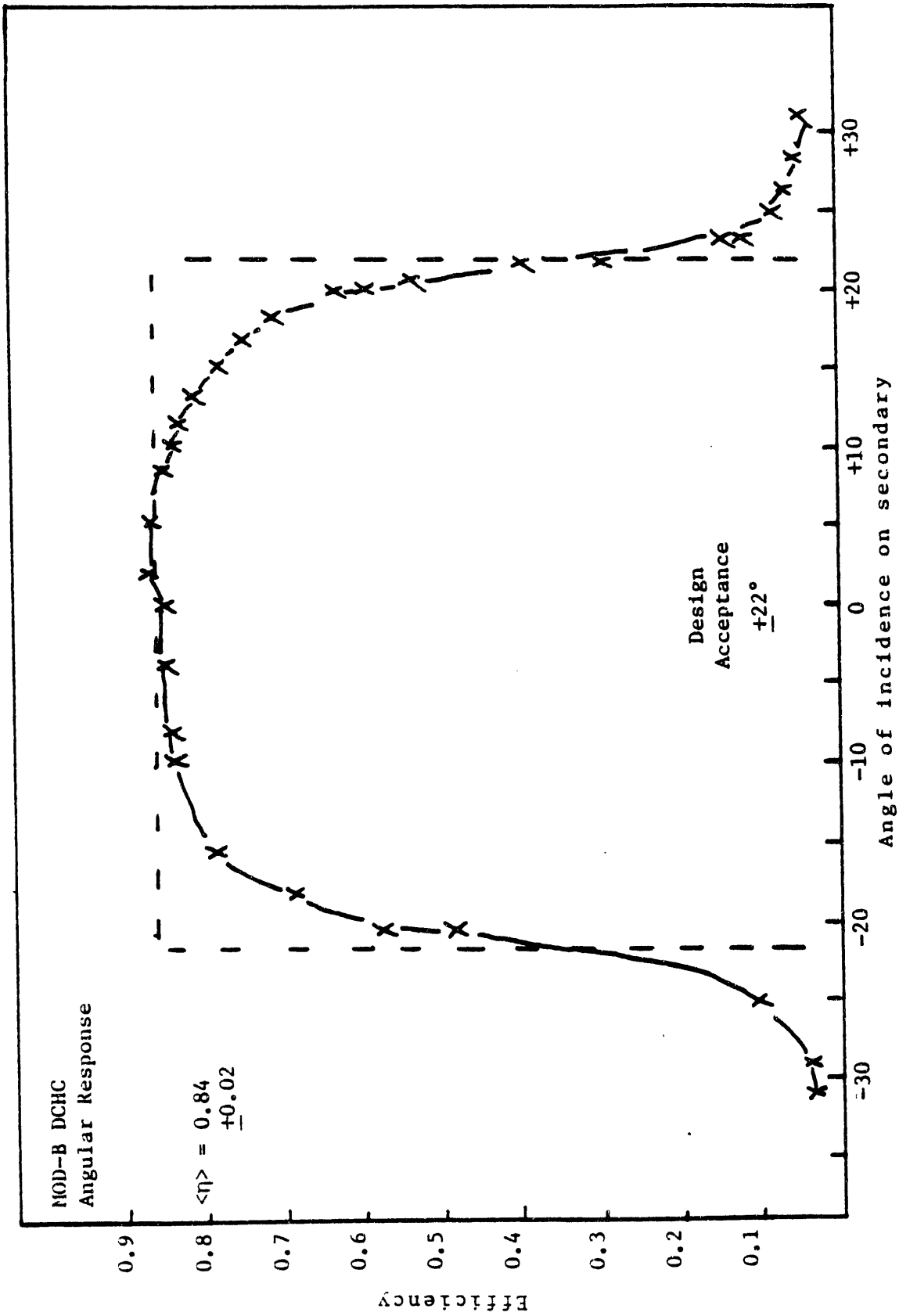

Figure 11. Measured efficiency as a function of angle of incidence for the MOD-B secondary

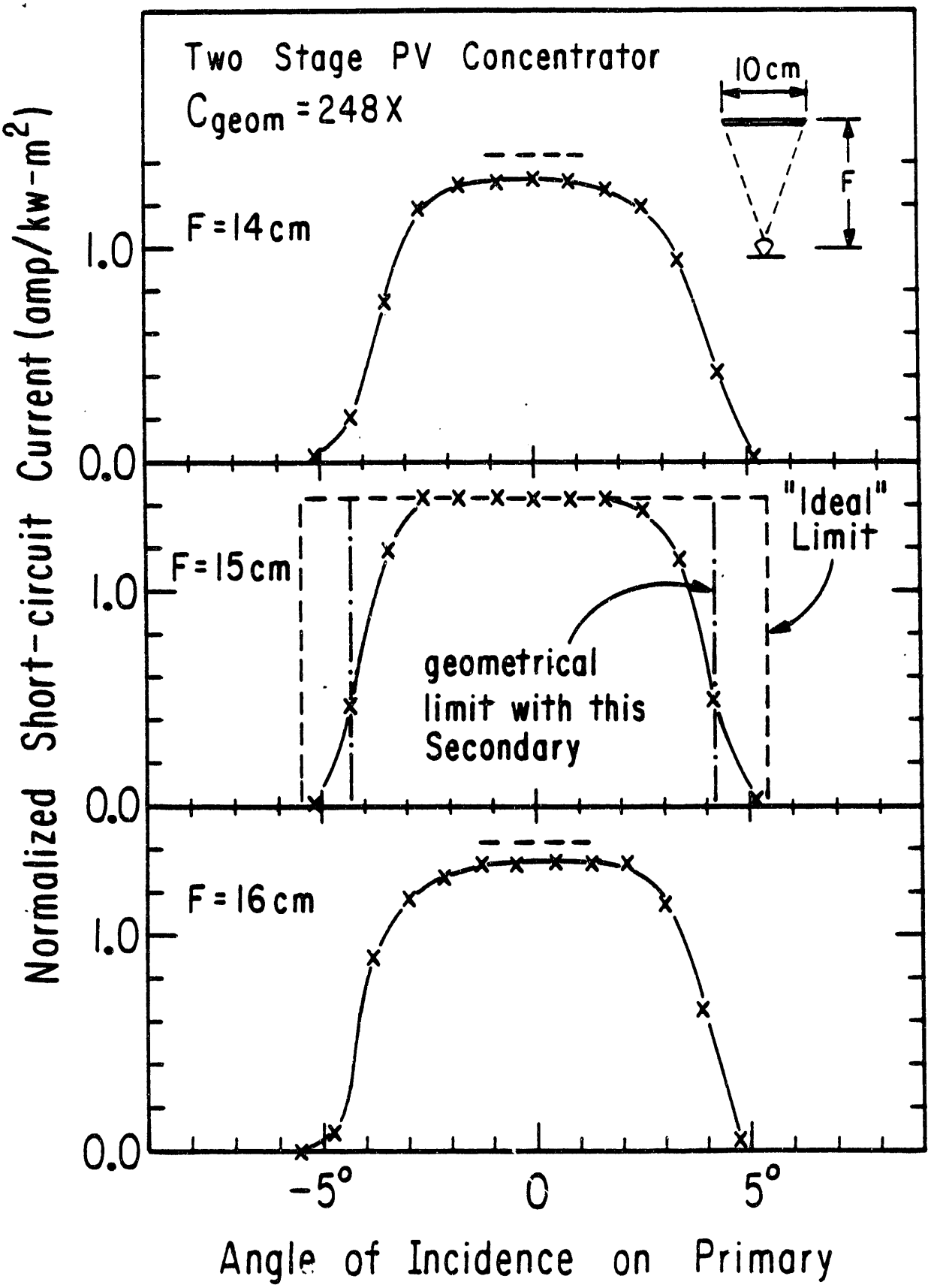

Figure 12. Measured angular response function for the full two-stage MOD-A prototype

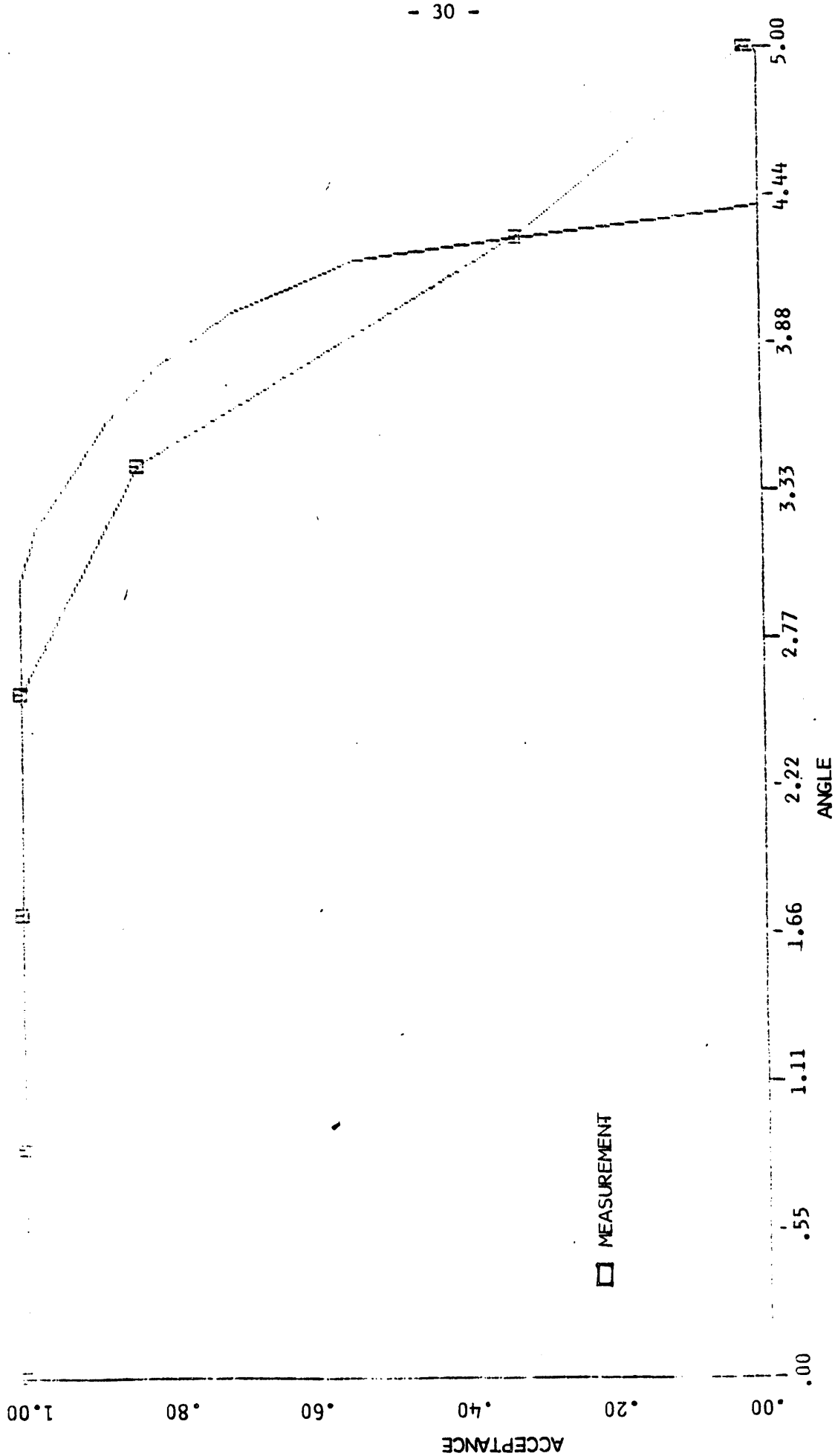

Figure 13. Ray trace calculation of the throughput (normalized to unity) as a function of angle of incidence relative to the primary normal compared with the observed shape

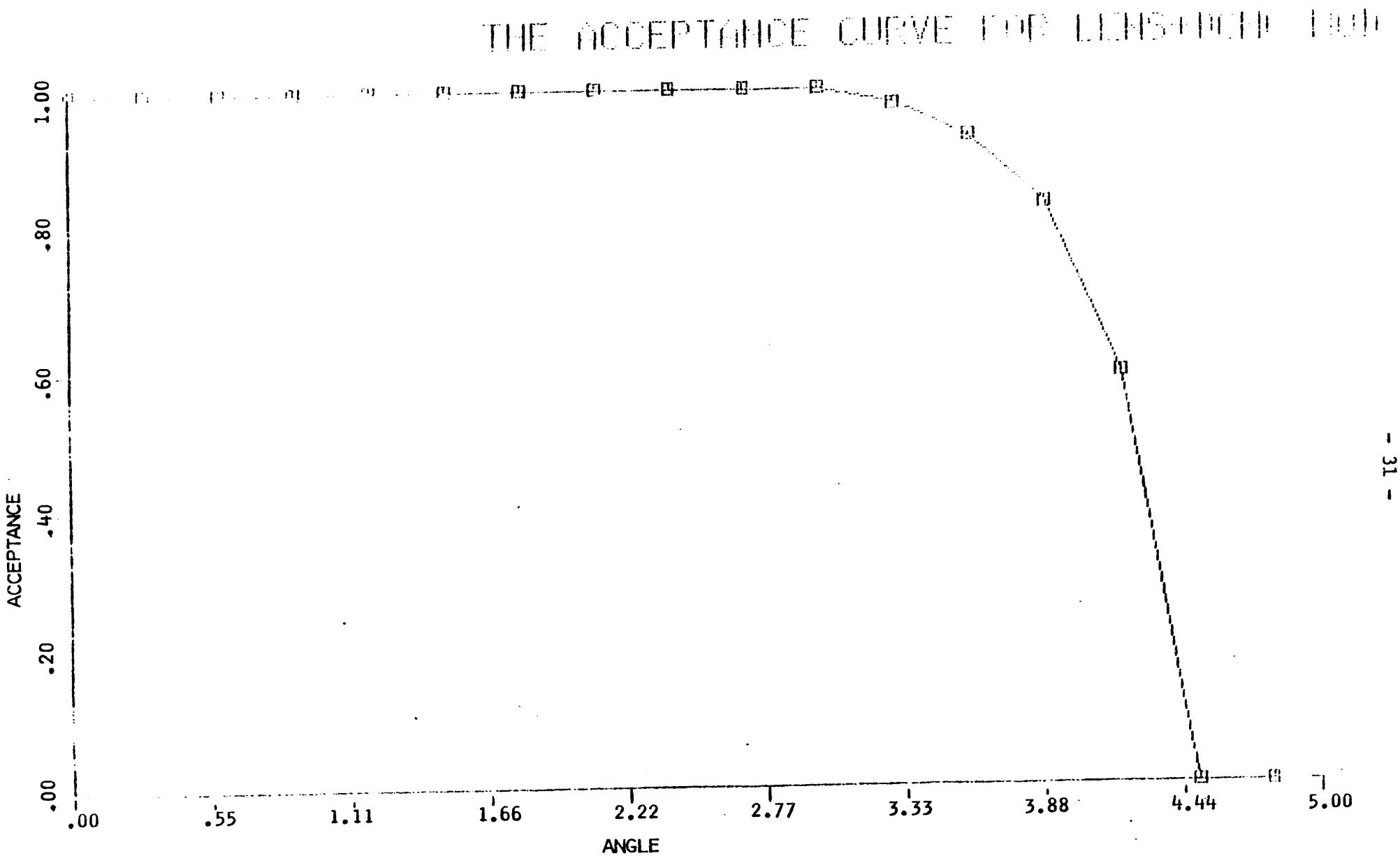

Figure 14. Ray trace calculation of the throughput versus angle for the full MOD-B configuration

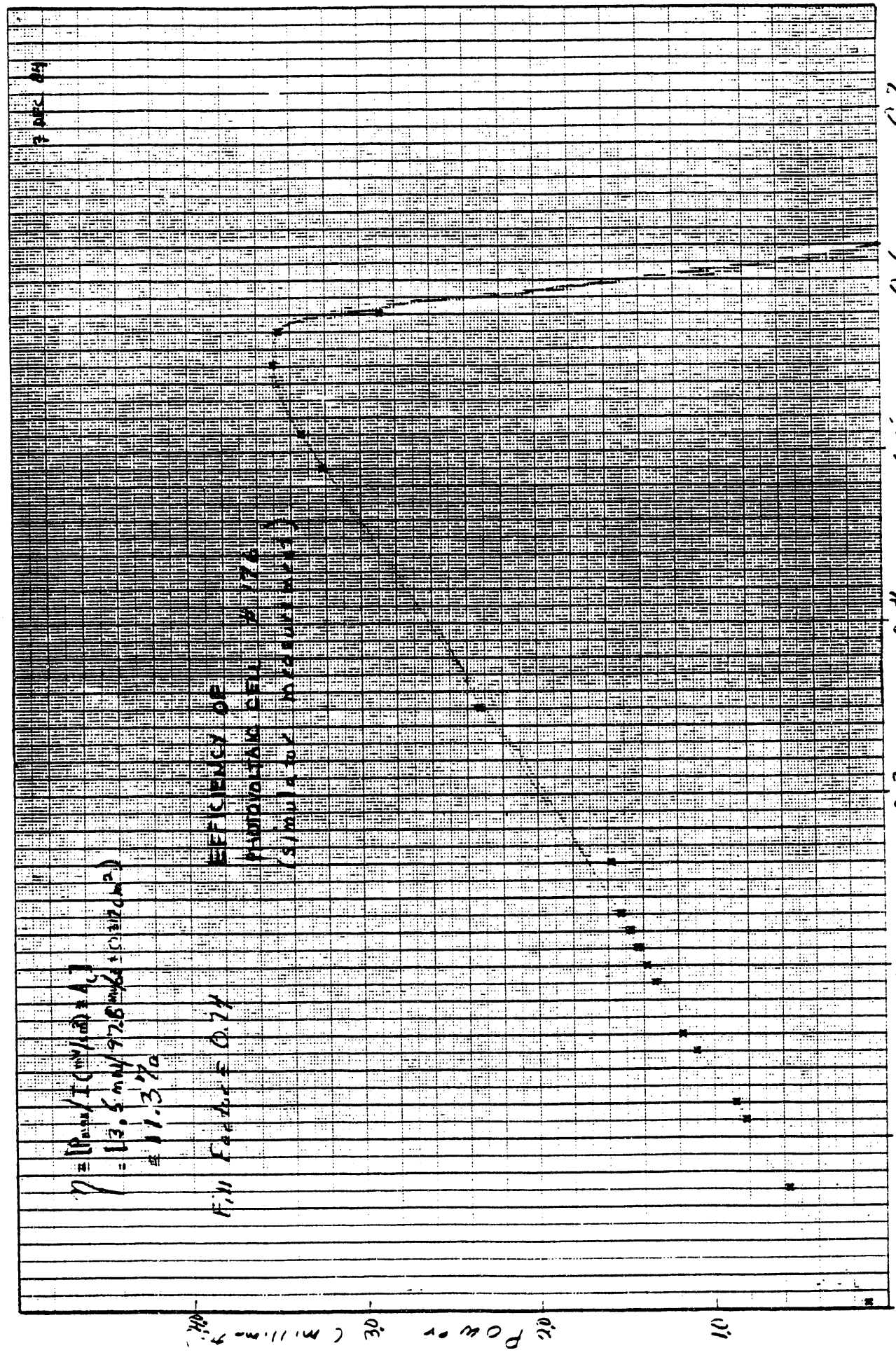

Figure 15. Power versus voltage curve for one of the Microwave cells under one simulator sun

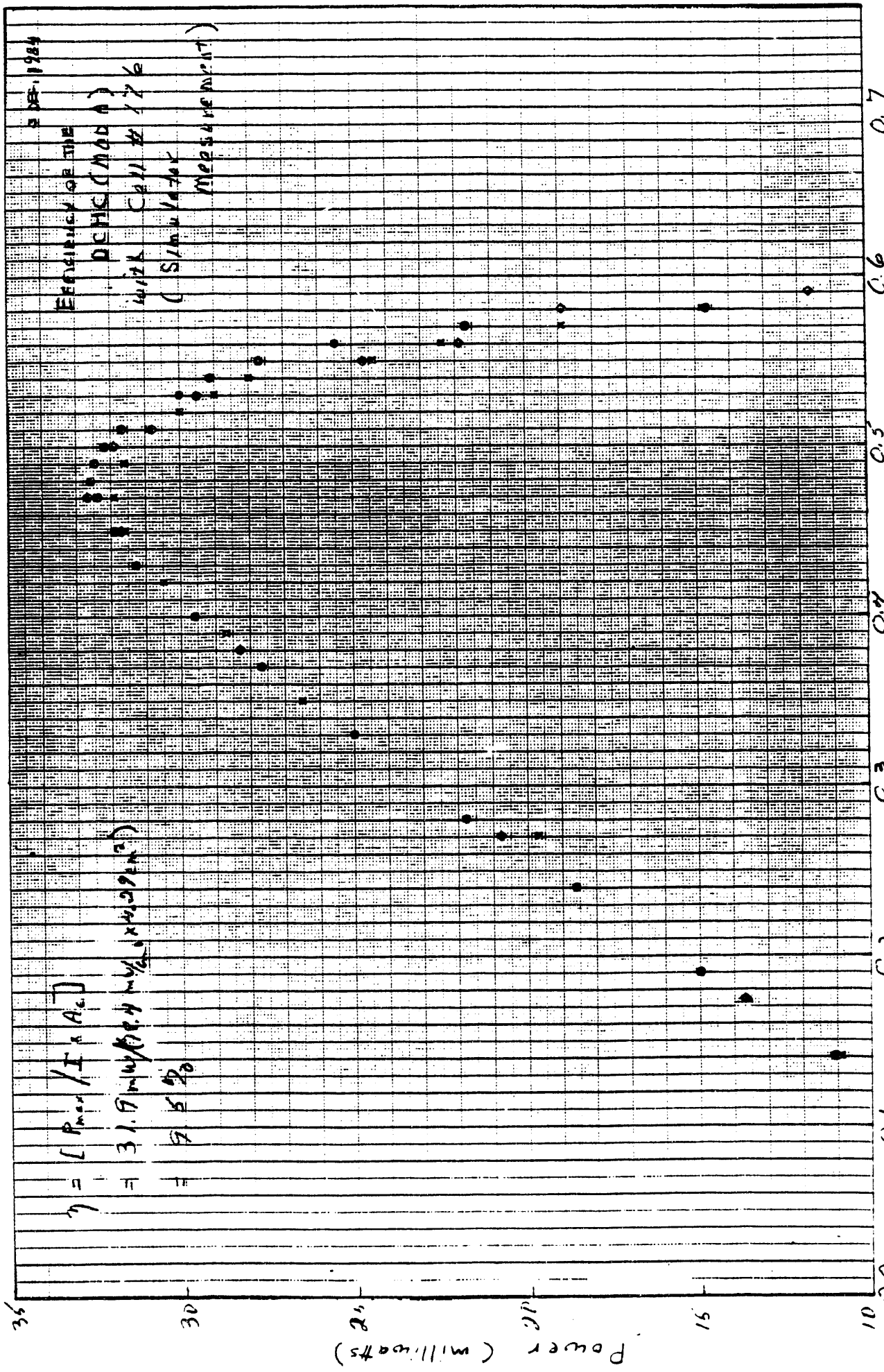

Figure 16. The power voltage curve for a secondary (C_2 = 13.5X) cell combination under the solar simulator

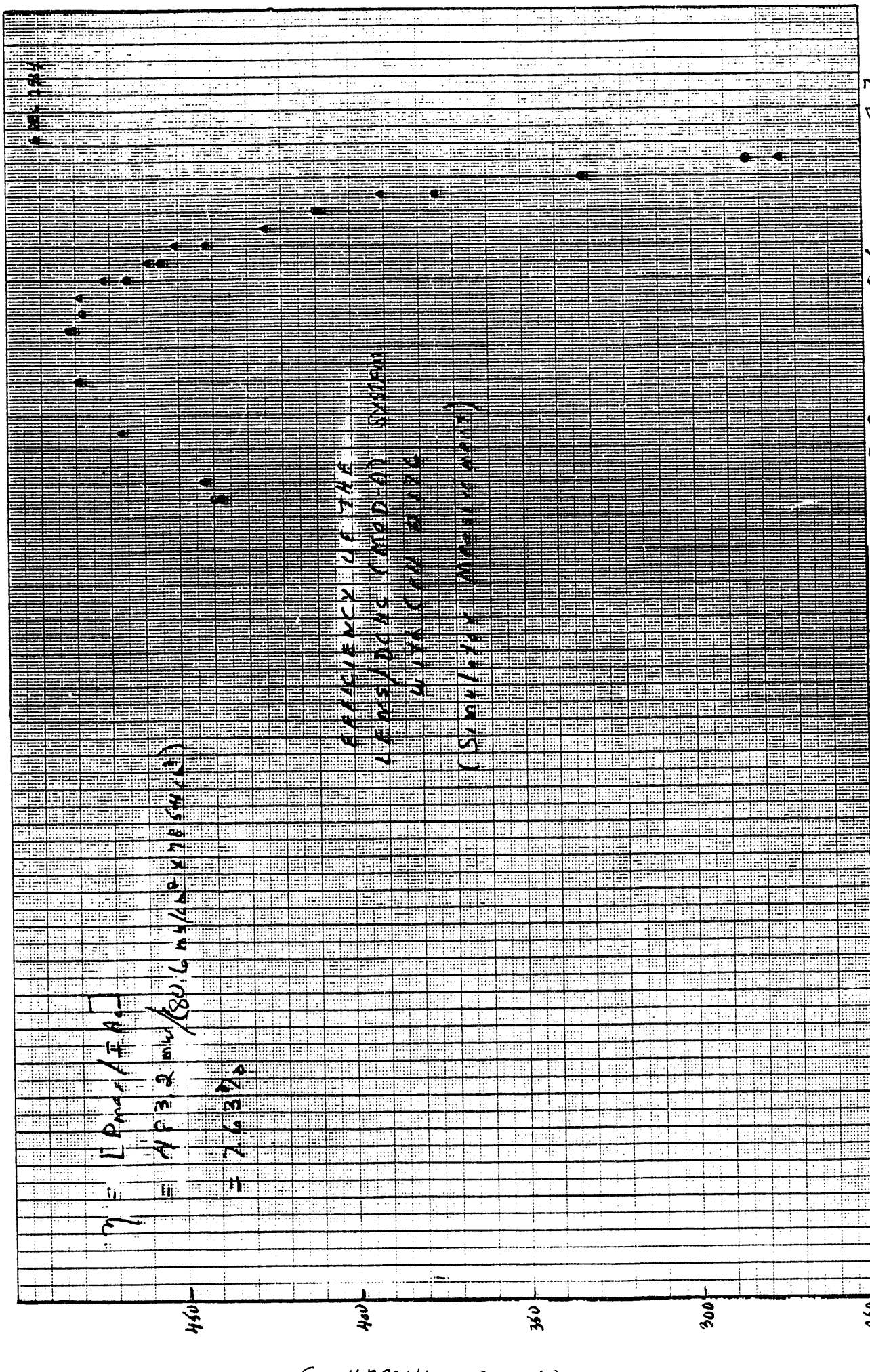

Figure 17. Simulator measurement of the full concentrator power output. Correction for losses due to simulator divergence has not been made

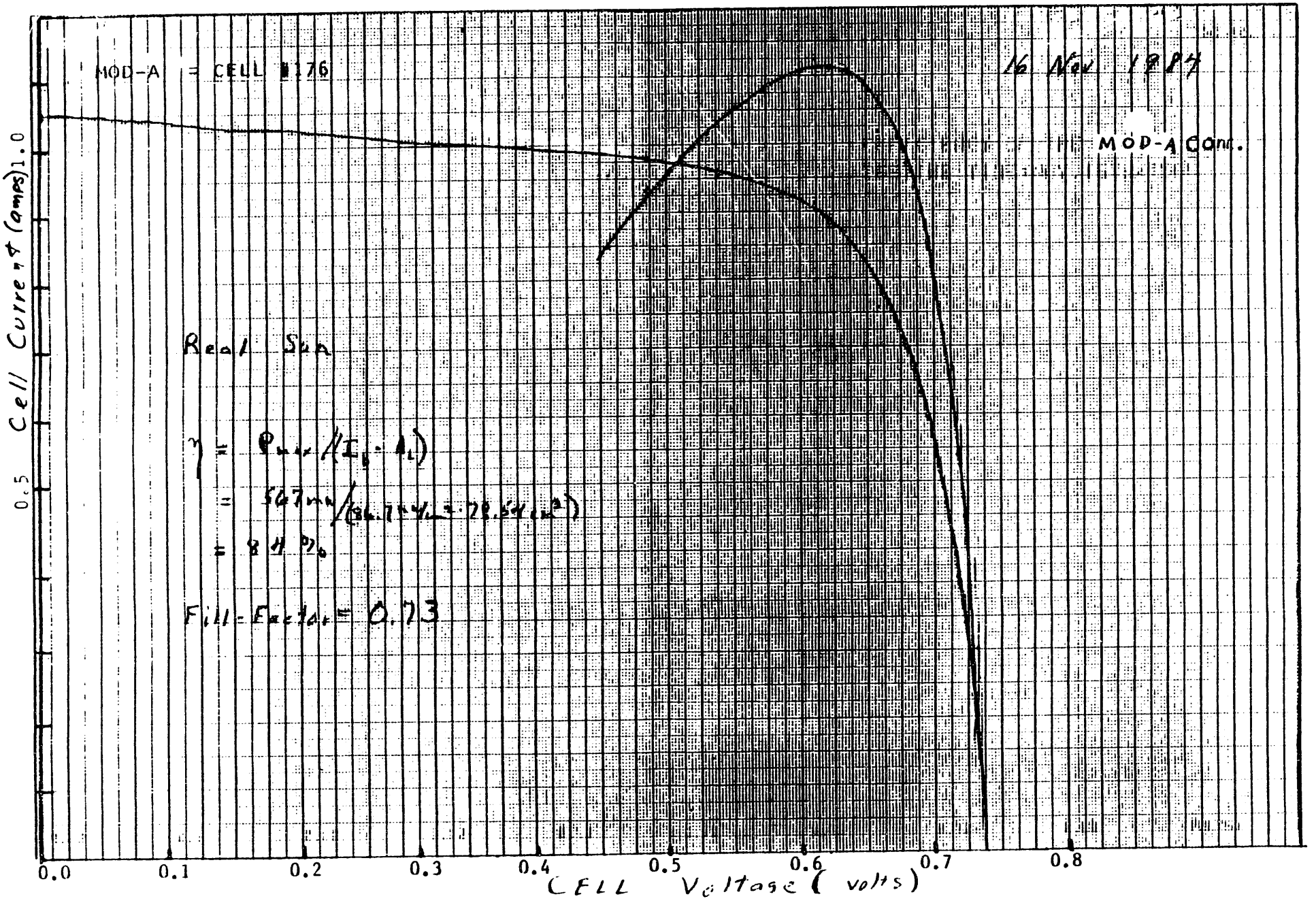

Figure 18a. Current-voltage and power voltage responses for the full MOD-A concentrator

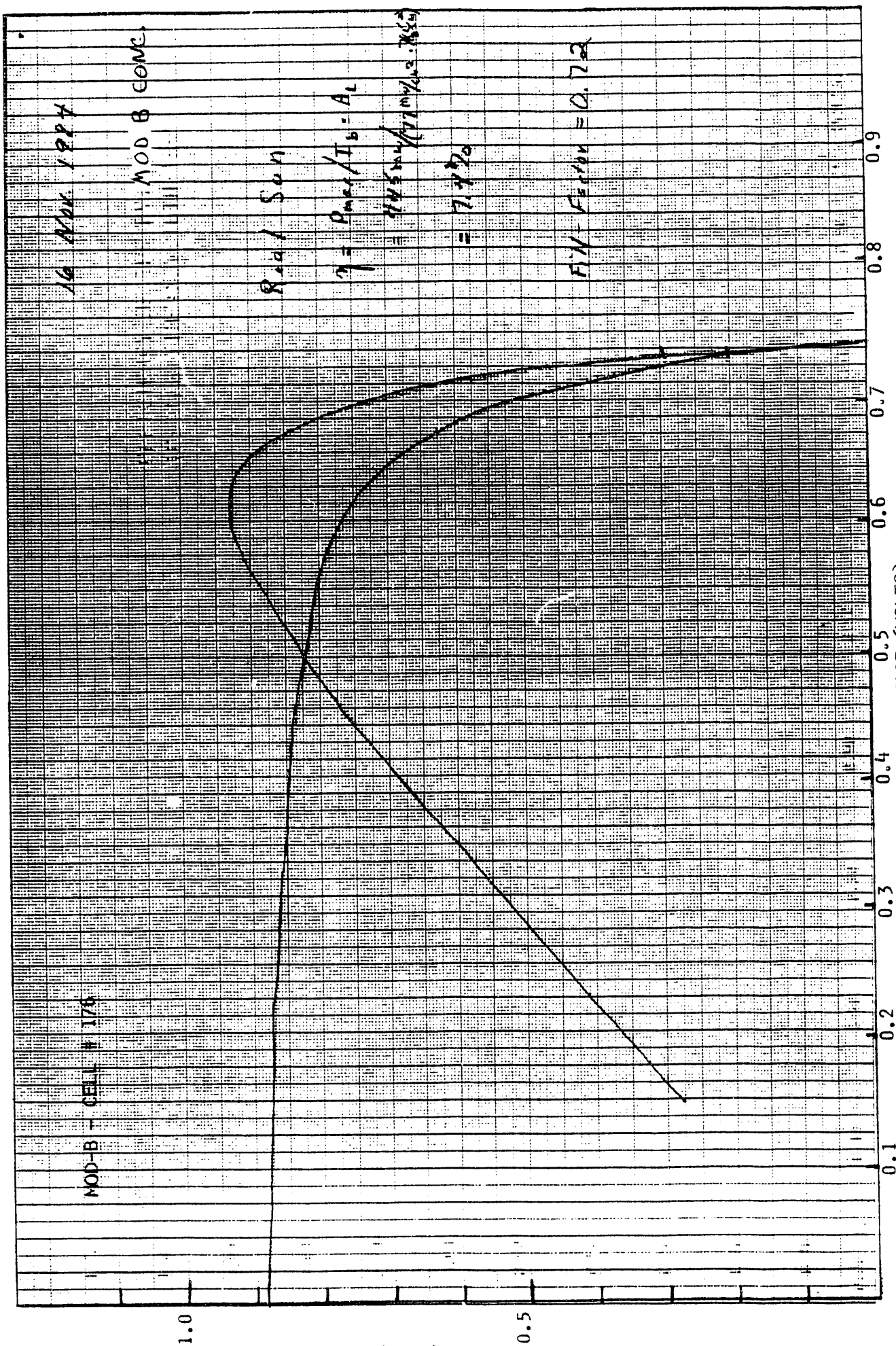

Figure 18b. Current and power versus voltage for the MOD-B configuration

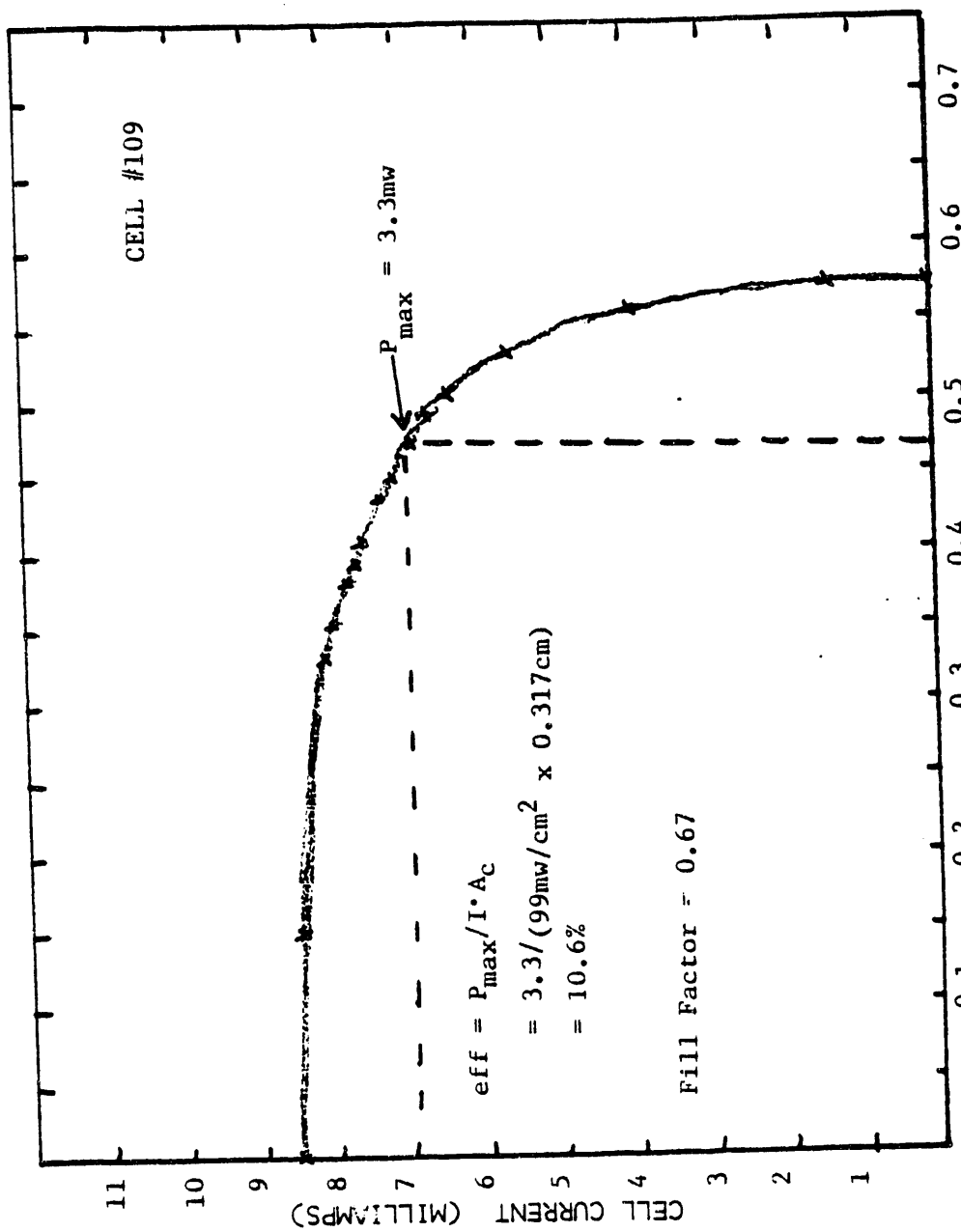

Figure 19a. Current voltage characteristic for one of the Microwave cells under one (real) sun

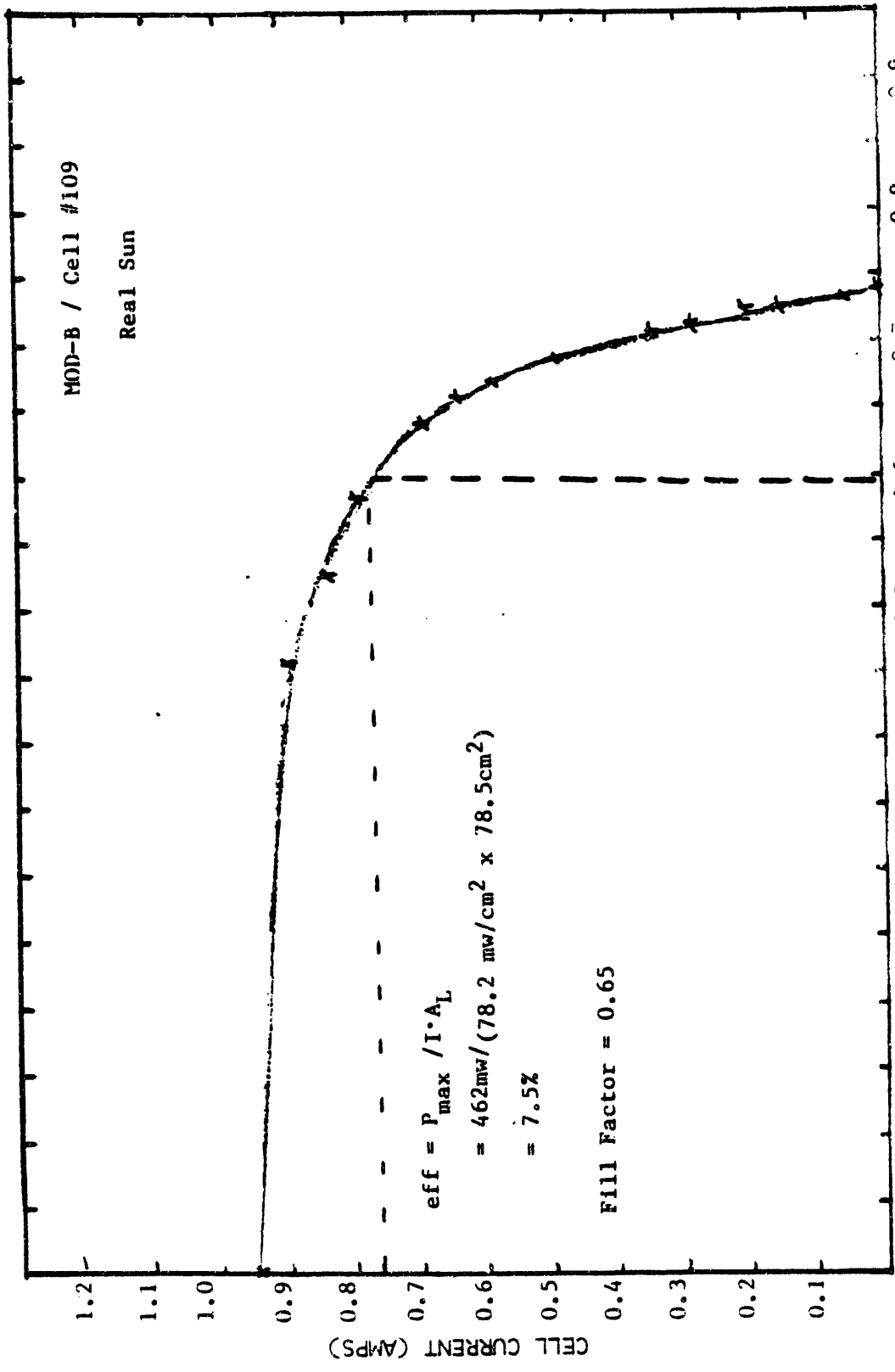

Figure 19b. Current voltage characteristic for the full MOD-B configuration

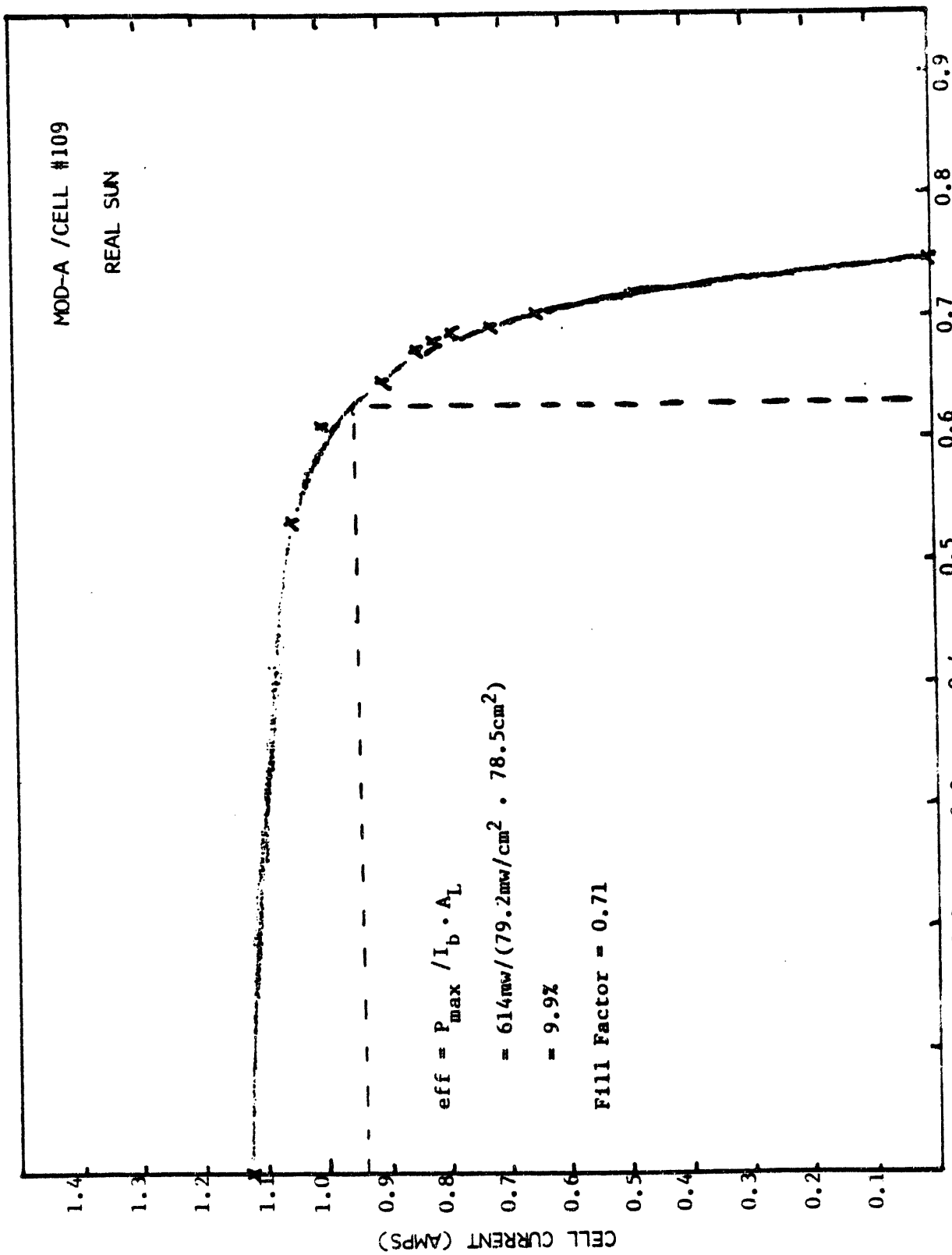

Figure 19c. Current-voltage characteristic for the full MOD-A configuration

END

DATE FILMED

12/22/92